

Bladed Disks: Flutter

Roque Corral

Industria de Turbopropulsores S.A.
28830 San Fernando de Henares, Madrid

January 25, 2012

Abstract

The basic concepts of bladed-disk dynamics and flutter are reviewed. First an introduction to the engineering problems related with flutter and its classification is given, then we review the basics of bladed-disk dynamics and unsteady aerodynamics for turbomachinery. Finally the tuned flutter problem is formulated and the problem of its computation affordable computations is addressed. The main objective is to make the reader aware of the physical origin of the concepts and their implications but not to provide design rules that could be readily applicable to particular designs.

1 Introduction

Dynamic Aeroelasticity

Elastic and aerodynamic forces interact between them to construct the discipline that is known as aeroelasticity. When unsteady effects are retained then aeroelastic effects are referred to as dynamic. There are three quite different aeroelastic phenomena, namely, forced response, aerodynamic instabilities and flutter. The objective here is to review these three concepts to focus afterward in the aeromechanic instability termed as flutter. Flutter may occur in different components, we will restrict ourselves here to bladed-disk flutter although it is possible to see flutter in other components with or without cyclic symmetry such as rotating seals, panels or vane packets for instance.

Forced Response

Forced response of blades is due to the synchronous aerodynamic excitation of neighbouring blade-rows. These excitations may be due to the upstream wake velocity defects (vortical perturbations) and/or to inviscid potential pressure waves from either the preceding or following rows. Hot streaks caused by combustor cams may give rise also to vortical and entropy perturbations. The excitation frequency is associated with the blade passing frequency and its higher or lower harmonics. The response occurs only at the crossings of the excitation frequency with the natural frequencies of the bladed-disk for which the bladed-disk are responsive due to the matching of the circumferential wave-length of the mode-shapes and the excitations, in other words for those modes for which the excitation order is the same than the nodal diameter.

Figure 1 (left) sketches how wakes coming from the preceding row impinge in the rotor and give rise to unsteady forces. On the right strain gage measurements of a bladed-disk subject to a clean forced response are plot. The experimental Campbell diagram shows the presence of different modes represented by dark quasi-horizontal lines and their excitation by several engine orders.

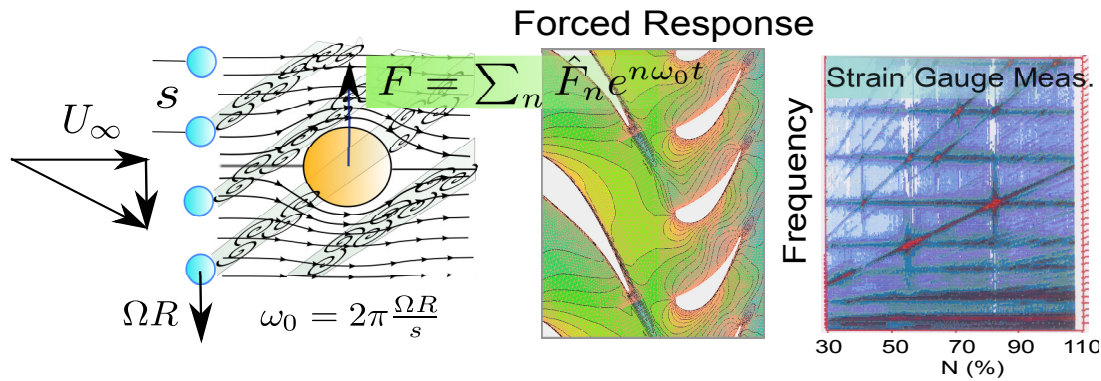


Figure 1: SCHEME OF THE FORCED RESPONSE WORKING PRINCIPLE. LEFT: CONCEPTUAL SCHEME. MIDDLE: ACTUAL FR CASE. RIGHT: EXPERIMENTAL CAMPBELL DIAGRAM.

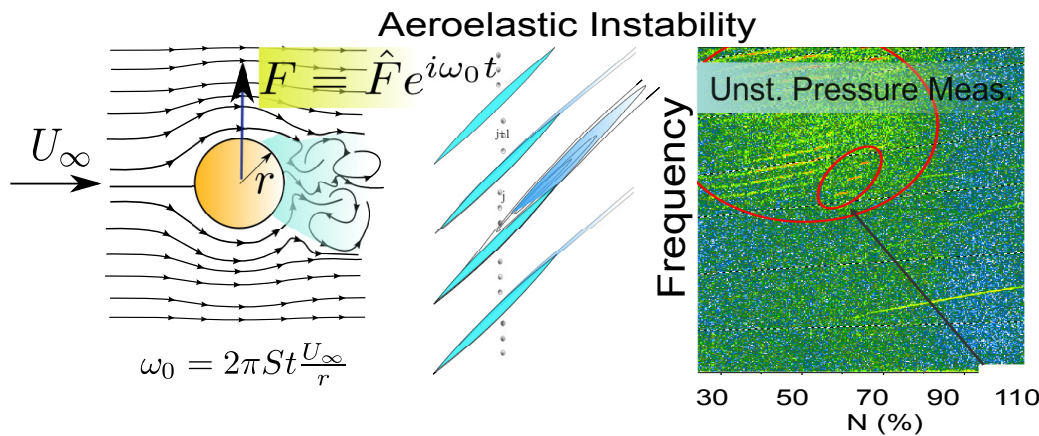


Figure 2: SCHEME OF THE AERODYNAMIC INSTABILITY WORKING PRINCIPLE

Aerodynamic Instability

Aerodynamic instabilities do not require contribution of neighbouring blade-rows. The aerodynamics may become unstable and cause unsteady perturbations. The simplest case is the vortex shedding behind a cylinder. The flow separates in the rear part due to adverse pressure gradient in the cylinder forcing the separation and oscillation of the flow with a well defined frequency range, ($St = \omega d/U_\infty \simeq 0.2$). This frequency does not correlate with the shaft speed of the engine and the excitation is referred to as non-synchronous. Vortex shedding due to the airfoil trailing edges is just a conceptual model of the origin of the physical problem but it is not a problem in practice since the excitation frequency is very high since $d/c \ll 1$. Engineering problems that fall under this category are rotating stall and buffeting for instance.

Frequency excitation does not happen at pure tones but has a broadband contribution. This may be seen in figure 2 (right) where unsteady pressure measurements due to rotating stall are displayed. It may be appreciated the existence of several bands, not correlating with the shaft speed. The dynamic pressure associated to these instabilities is of the order of the dynamic head and therefore the forces involve are usually very high. However the response is not always visible since this depends on the coincidence with a resonance.

Flutter

Flutter is defined as a blade response due to an asynchronous aeroelastic instability of isolated airfoils. In the same line that aerodynamic instabilities the presence of neighbouring blade-rows is not needed. The main difference here is that the airfoil motion is needed to develop an unstable behaviour, in other words while buffeting and rotating stall is a pure aerodynamic instability flutter is an aeroelastic stability that requires the participation of the structure.

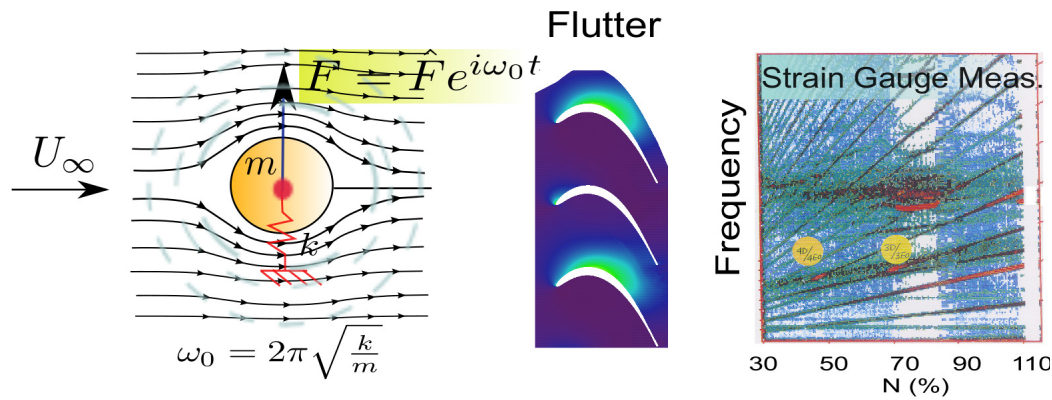


Figure 3: SCHEME OF FLUTTER WORKING PRINCIPLE

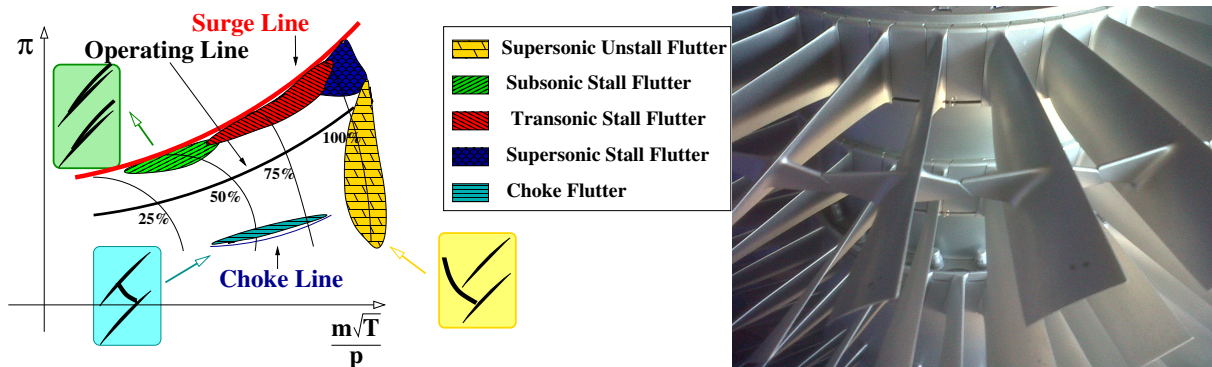


Figure 4: CLASSICAL FLUTTER COMPRESSOR MAP (LEFT) AND COMPRESSOR SNUBBERS USED TO PREVENT FLUTTER

Frequency response is necessarily associated to structural modes since their participation is needed. Figure ?? emphasizes that the instability may develop in a purely inviscid flow without any kind of separation, but the instability requires the presence of the structure. On the right the strain gage measurements of a fluttering bladed-disk may be seen. Flutter creates high response along several points usually of the speed-line that do do coincide with any synchronous response. The modulus of the unsteady pressure scales with the vibration amplitude on the contrary than in a pure aerodynamic instability.

Phenomenological Classification and Description

Flutter is primarily seen in in fans, front and middle compressor blades and high aspect ratio low-pressure turbines. Flutter is not a concern for HPT since the are made of thick, low aspect ratio blades. The types of flutter observed in compressor blading are usually displayed in a compressor map (see Fig. 4). Flutter does not occur usually near the design point where compressor airfoils are operating close the nominal incidence, but at off-design conditions. The most common type of flutter is stalled flutter that is seen in fans and front compressor stages. A standard design criterion is to require that the flutter margins is high enough to avoid it in all the operating range, however with the recent improvements in surge margin today is difficult to provide enough flutter margin to handle engine-to-engine variation and deterioration.

Supersonic unstalled flutter is easily seen in shrouded fans, however the design of shrouded fans is not a modern design practice. This type of flutter tends to occur at climb conditions close to the maximum corrected speed. Choke flutter is much less common and it is restricted to rear compressor stages.

Low-pressure turbine flutter may be detected in any high aspect ratio, H/c , rotor blade or vane. Flutter is detected in a wide envelope of the turbine operating range, but the most critical point is associated to Maximum Take-off conditions where both the mechanical shaft speed and the turbine inlet pressure reach their maximum.

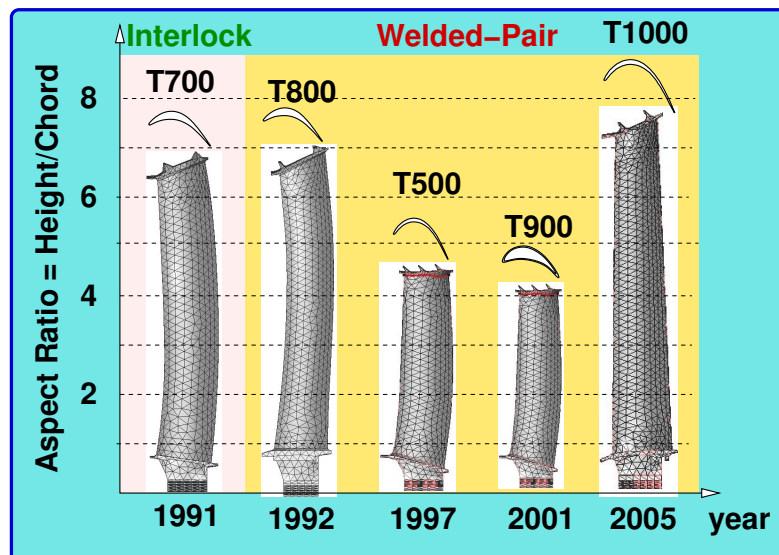


Figure 5: EVOLUTION OF LPT ROTOR BLADE ASPECT RATIO

Flutter occurred in early cantilever LPT designs (1F) on Pegasus, RB145, etc. during the development phase, the fix was based in adding lacing wires or shrouds. Plain sided shrouds which had clearance at operating conditions fluttered as well in 1st flexural modes (Dart and Conway engines). The move to interlock shrouds, supposed to remain tight throughout the running range, gave rise to vibration characteristics similar to the ones encountered in snubbed fans that gave rise to flutter of complex modes.

Figure 5 displays the rotor blade aspect ratio evolution of a family of large civil aeroengines. It may be seen that in the early 90's relatively large aspect ratio were designed and manufactured and that the interlock configuration, where the rotor blades are supposed to remain in tight contact during the whole flight envelope was abandoned in favour of cantilever blades welded-in-pair. The ultimate goal of welding the rotor blades in pairs was to mitigate flutter effects by providing additional aerodynamic damping. The drop and raise of the aspect ratio with time is associated to a combination of development problems in previous designs, change of design targets and improvements in prediction methodologies based in a more intensive use of simulation tools.

Design limitations associated to the Flutter of NGVs in the last stages of LPTs are not uncommon, Compressor and turbines vanes are grouped in packets to reduce manufacturing costs. The number of vanes per packet ranges between 3 and 10. Flutter of vanes packets has unique ingredients since vane packets include modes which are very close in frequency that may interact among them [1, 2].

Mathematical Classification

Flutter may be classified also from a mathematical point view. This is interesting since it helps to determine the level of modelling that it is required for each problem. **Classical flutter** is encountered when just a single well separated unstable mode is encountered and the aerodynamics is linear since there are not highly non-linear phenomena, such as shock waves or separation. The perturbed unsteady flow may be considered as a small perturbation of the mean flow and may be computed using linear methods. This type of flutter may be seen in subsonic low-pressure turbines and compressors.

Non-linear flutter happens for single-mode non-linear aerodynamics. Most, if not all, fan and compressor flutter types fall under this category. Choke and supersonic unstart flutter features shock waves that are responsible of the instability. Stall flutter is based in the presence of large vortices and separated

regions interacting with the structure. Their simulation require non-linear aerodynamic models but some engineering approaches based in linear analysis and experience are also possible.

Coalescence flutter refers to instabilities that are caused due to the interaction among several modes . The simplest case is the classical bending-torsion interaction that may be see in aircraft wings. The existence of coalescence flutter requires the presence of high enough aerodynamic forces that may couple the purely structural modes. Bladed-disks are designed to have separated mode families in terms of frequency but there are cases in which this interaction is unavoidable like in vane packets where several structural modes with nearly the same frequency may be found. Low density bladed-disks like fans and propfans may experience coupled flutter due to frequency corrections due to aerodynamics effects.

Classical Flutter

The main hypotheses involved are that the flow remains attached to the airfoil and the instability is induced solely by the phase difference between the structure motion and the induced aerodynamics forces. Another implicit hypothesis is that a single mode is involved because different modes are well apart in terms of frequency, we will expand this issue latter on to properly define the concept of separated modes. Bladed-disk flutter add another particularity, namely that the different airfoils of the bladed-disk interact aerodynamically among them. As it has already been mentioned this type of flutter may be seen in intermediate- and low-pressure turbines

Classical flutter may be readily understood analysing whether the flow extract or communicate energy to the airfoil. The standard form of looking at this problem is calculating the **work-per-cycle** performed by the fluid ion the airfoil that may be expressed as

$$W_{cycle} = \int_0^T \int_{\Sigma_{blade}} p \mathbf{V}_{blade} \cdot \mathbf{dA} dt \quad (1)$$

if neither the velocity of blade, $\mathbf{V}_{blade}(t)$, nor the pressure on the airfoil surface, depend on the airfoil position then the work per cycle reduces to

$$W_{cycle} = \int_0^T \mathbf{V}_{blade}(t) \cdot \mathbf{F}(t) dt. \quad (2)$$

Let us assume that the blade undergoes an harmonic motion, $\mathbf{x}_{blade} = \mathbf{x}_0 \sin \omega t$, thus the blade velocity is $\mathbf{V}_{blade} = \omega \mathbf{x}_0 \cos \omega t$, and that the blade force leads its displacement by an angle ψ , i.e. $\mathbf{F} = \mathbf{F}_0 \sin(\omega t + \psi)$ then the work-per-cycle is

$$W_{cycle} = \omega \mathbf{x}_0 \mathbf{F}_0 \int_0^{2\pi/\omega} \cos \omega t \sin(\omega t + \psi) dt = \pi \mathbf{x}_0 \mathbf{F}_0 \sin \psi \quad (3)$$

If $\psi > 0$, the structure absorbs energy from the flow and the system is unstable. It is important to highlight that flutter depends solely in the phase between the airfoil displacement and the aerodynamics force.

Another form of looking at the problem is by representing the forces and displacements in the complex domain. In this case $W_{cycle} = \text{Re}(\hat{F}\hat{v}) = \text{Re}(\hat{F}i\omega\hat{x}) = -\omega x_R F_I$, and therefore the sign of the work is controlled by the imaginary part of the force which is nothing that the phase between the force and the displacement.

The relationship between the work-per-cycle and the phase is illustrated in figure 6. If a force is applied on the airfoil and as a consequence the airfoil is displaced a positive work is performed and the structure absorbs energy. If forces and displacements are exactly in phase ($\psi = 0$) or anti-phase ($\psi = \pi$), the system is conservative and the work dissipated per cycle is null.

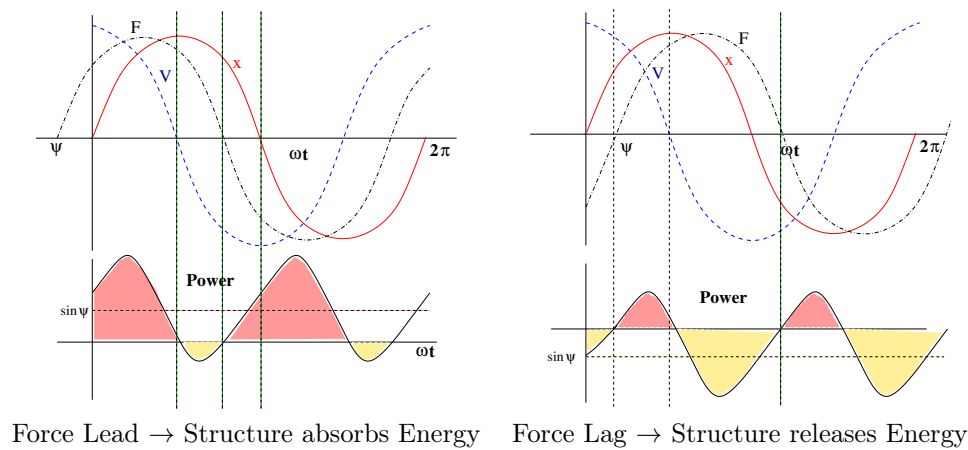


Figure 6: WORK-PER-CYCLE FOR TWO DIFFERENT PHASING BETWEEN THE FORCE AND THE DISPLACEMENT

2 Bladed-Disk Dynamics

A simple model is presented to describe the key elements of bladed-disk dynamics. Different asymptotic limits are analysed to obtain analytical description of some of the more well known behaviours

Introduction

Linear bladed-disk dynamics is computed today routinely by gas turbine manufacturers using finite element methods. Complex blade shapes and disks are discretised using automatic grid generators, the governing equations are written in discrete form and the eigenvalue problem of set of ordinary differential equations solved to obtain the natural frequencies and the mode-shapes. Frequencies are needed to relate them with the shaft speed and construct Campbell diagrams and mode-shapes to derive aerodynamic damping and alternate stresses. The third building block of the bladed-disk dynamics, namely, the modal damping may not readily derived from FE computation and will not be addressed here.

Rotor blades are coupled with their neighbours via the structural connections that inevitably exists either through the disks, the casings in the case of stator vanes, or through the shroud rings that are included to stiffen the assembly. The structural coupling among different rotor blades significantly influences the natural frequencies and mode-shapes of the assembly and need to be retained in the simulations. Analysis including just a single blade must be regarded as first step in the simulation process.

Perfectly tuned bladed-disks exhibit cyclic symmetry. This means that the whole wheel may be split in N identical sectors, probably containing several airfoils as it is always the case for sectorised vanes, and impose cyclic boundary conditions in the periodic boundaries to reduce the computational domain from the whole wheel to a single sector largely reducing the computational time require to solve the problem.

Bladed-Disk dynamics has been well reported. Here our interest here is to make a very short review of the underlying concepts resorting to a simplified lumped model that contains all the key ingredients.

Disks, or any continuous structure with cyclic-symmetry vibrate in double nodal diameters (see Figure 7). Nodal diameters are the locus of the points with zero displacement that traverse radially the disc. Mode-shapes with more nodal diameters have higher natural frequencies since the mode is stiffer. As the excitation frequency increases the disk may exhibit nodal circles which are points at constant radius with zero displacement.

Bladed-Disks are constructed fixing rotor blades to a disk, either using fir-tree or dove tail attachments, or welding the rotor blades to the disk or even machining integral parts with disks and blades as it is usually the case in small compressors (Blisks). In any case with a large degree of generality it may be

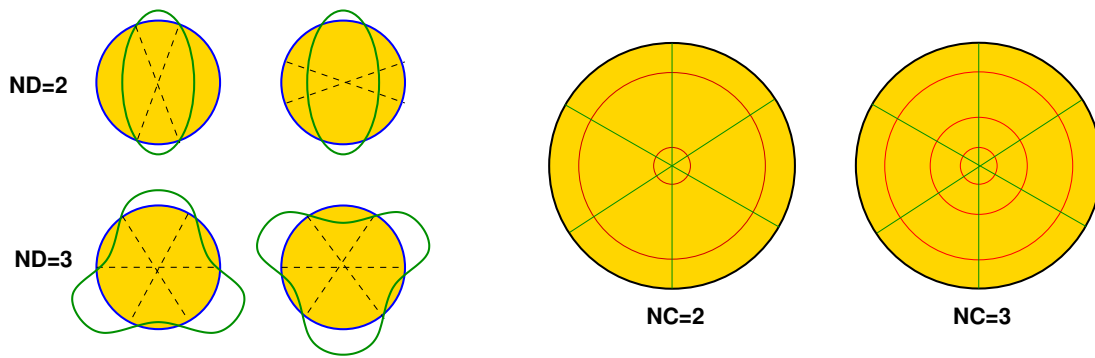


Figure 7: SKETCH OF DISK MODE-SHAPES. LEFT: NODAL DIAMETERS. RIGHT: NODAL CIRCLES

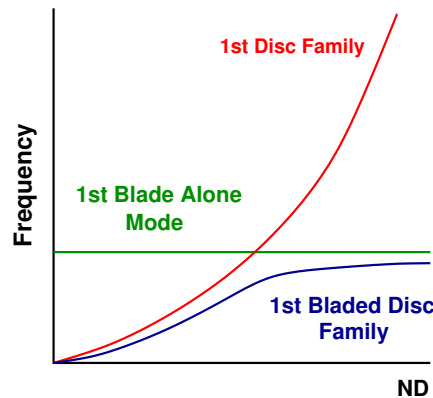


Figure 8: SKETCH OF THE NATURAL FREQUENCIES OF A BLADED-DISK AS A FUNCTION OF THE NODAL DIAMETER

stated that for very stiff disks the lower natural frequencies are dominated by blade-alone modes, i.e.: modes which are very similar to those that can be obtained clamping the rotor blade at the root, while for flexible disks the rotor blade and the disk modes may interact.

Figure 8 displays the frequency versus the nodal diameter of a generic bladed-disk. The horizontal frequency represents the frequency that would be obtained by clamping the rotor blade at the attachment that does not depend on the nodal diameter since the disk is not included in the representation. The parabola-like curve represents the natural frequencies of the disk alone, that increase with the nodal diameter. The blend between these two curves is the bladed-disk 1st family of modes. It may be observed that for low nodal diameters the system is dominated by disk modes, while for high nodal diameters the bladed-disk natural frequencies corresponds in first approximation with that of the rotor blade alone.

The questions that arises immediately are: What does exactly mean a rigid disk? or How flexible need to be a disk to see the disk dynamics? or How high need to be a nodal diameter to see just the rotor blade dynamics? We will try to answer this question by looking at a simplified bladed-disk model.

Figure 9 show the frequency versus the nodal diameter of a low-pressure turbine real bladed-disk computed using a FE model. Several families of the assembly are plot, but it may be seen that all of them have the same structure that that sketch in figure 8. Low nodal diameters correspond to long wave-length modes while high nodal diameters have short wave-length and essentially the same frequency. This structure of the purely structural eigenvalues applies to any kind of bladed-disk.

Bladed-Disk Lumped Model

A tuned bladed-disk formed by a disk and a set of rotor blades attached to it, may be represented from a conceptual point of view as a ring on N identical masses, M_d joined by a spring of stiffness, k_d that

The characteristic equation providing the eigenvalues is thus:

$$\mu\tilde{\omega}^4 - \left[(\mu + 1) + 4\kappa \sin^2 \frac{n\Delta\theta}{2} \right] \tilde{\omega}^2 + 4\kappa \sin^2 \frac{n\Delta\theta}{2} = 0 \quad (8)$$

The natural frequencies of the problem depend therefore of three parameters:

$$\frac{\omega_n^2}{\omega_{blade}^2} = f \left(\mu = \frac{M_{disk}}{M_{blade}}, \kappa = \frac{K_{disc}}{K_{blade}}, \Theta = n\Delta\theta = 2\pi \frac{n}{N} \right) \quad (9)$$

the disk to blade mass ratio, μ , the disk to blade mass stiffness, κ , and the non-dimensional wave number or nodal diameter, Θ . Equation 8 is a second order algebraic equation in $\tilde{\omega}^2$ that can be solved analytically but it is more interesting to look at some asymptotic limits.

Mathematical and Physical Interpretation

There are a number of consequences that may be derived from the mathematical structure of the problem that have their physical counter part.

1. First of all all the eigenvalues, $\tilde{\omega}^2$, of the model problem are real. This may be readily seen by noting that the characteristic equation 8 is a second order equation of the form $\tilde{\omega}^4 - 2b\tilde{\omega}^2 + c = 0$ whose solution is $\tilde{\omega}^2 = b \pm \sqrt{b^2 - c}$. Since b and c are always greater than zero, and $b^2 > c$, then $\tilde{\omega}^2$ is always real and greater than zero. This physically means that the system is not damped and conserves the energy since the solution may be expanded in sines and cosines of constant amplitude according with Eq. 6.
2. The eigenvalues are double since Eq. 6 does not change for positive or negative nodal diameters or wave numbers, n . This means that from a purely structural point of view the system is symmetric. The wave-length of the waves is $\lambda = 2\pi/n$.
3. From a mathematical point of view the natural form of looking at the solution is as pairs of forward and backward travelling waves of wave-length λ and phase velocity $c = \pm\tilde{\omega}/n$

$$x(t) = A_n \cos(n\theta + \tilde{\omega}t) + B_n \cos(n\theta - \tilde{\omega}t + \phi)$$

however this solution may be recombined and expressed as two standing-waves, setting $\phi = 0$, of the form

$$x(t) = (A_n + B_n) \cos(n\theta) \cos(\tilde{\omega}t) - (A_n - B_n) \sin(n\theta) \sin(\tilde{\omega}t)$$

which is the standard form that FE packages provide the mode-shapes and laboratory experiments see bladed-disk assembly mode-shapes when they are excited in a stationary frame of reference.

Asymptotic Limits

To increase the understanding of this model problem let us consider the following asymptotic limits:

1. The disk is much heavier than the rotor blades, i.e.: $\mu \gg 1$
 - (a) $\kappa \sim 0(1)$ or $\kappa \ll 1$
 - (b) $\kappa \gg 1$

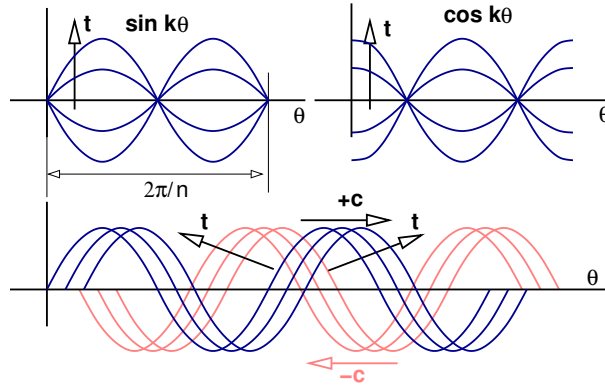


Figure 11: Sketch of standing- (top) and travelling-wave (bottom) solutions

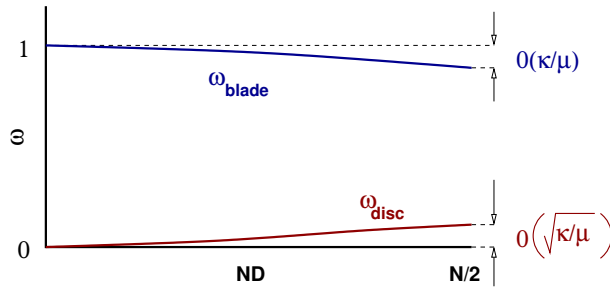


Figure 12: NATURAL FREQUENCY VS NODAL DIAMETER OF A BLADED-DISK WITH $\mu \gg 1$ AND $\kappa/\mu \ll 1$

2. Blade and disk masses are comparable, i.e.: $\mu \sim 1$

- (a) High nodal diameters $n/N \gg \kappa^{-1/2}$
- (b) Low nodal diameters $n/N \ll \kappa^{-1/2}$

Heavy and Relatively Flexible Disk

If the disk is much heavier than the blades ($\mu \gg 1$), the 0^{th} order dispersion relation reduces to $\mu\omega^4 - \mu\omega^2 = 0$, that basically means that the disk natural frequencies are very low, zero in first approximation, $\omega_{Disk}^2 = 0$, and the rotor blades natural frequencies correspond the blade-alone frequency, i.e.: $\omega_{Blade}^2 = 1$ in non-dimensional form. Disk and Blades frequencies are well apart and they do not interact among them. Rotor blade vibrates at its natural blade and the disc does not move. Next terms of the expansion are:

$$\omega_{Disk} = 2\sqrt{\frac{\kappa}{\mu}} \sin \frac{\Theta}{2} \text{ and } \omega_{Blade} = 1 - 2\frac{\kappa}{\mu} \sin^2 \frac{\Theta}{2}$$

and the corrections are small provided that $\kappa/\mu \ll 1$. This limit is not seen in practice since although disks of industrial gas turbines may be much heavier than the blades they are also stiff and $\kappa \sim \mu$.

Heavy and Stiff Disk

If the disk is much heavier and, consequently, stiffer than the rotor blades, $\mu/\kappa \sim o(1)$, the situation is a bit different. In the previous case disk dynamics decouples from the blade because their characteristic times were very different. Now this is not true anymore but the disc is very stiff and has an independent behaviour. In this case the approximate solutions are: $\omega_{blade} = 1$ and $\omega_{Disc} = 2\sqrt{\frac{\kappa}{\mu}} \sin \frac{\Theta}{2}$. The

approximate disc equation is now: $\frac{d^2x_j}{d\tau^2} = \frac{\kappa}{\mu}(x_{j+1} - 2x_j + x_{j-1})$ which is decoupled from the rotor blade dynamics.

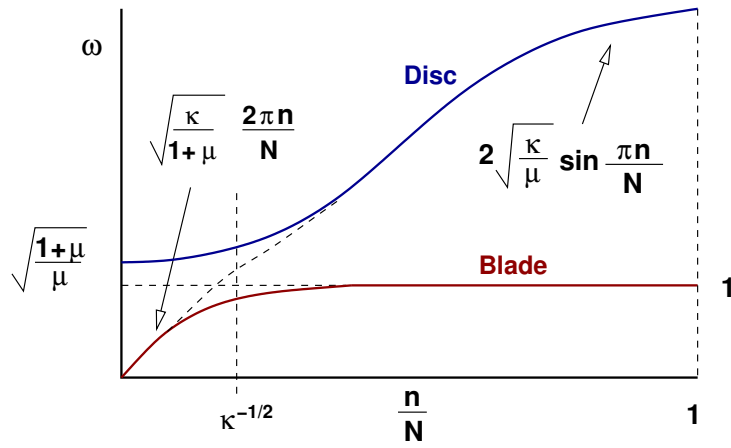


Figure 13: NATURAL FREQUENCY AS A FUNCTION OF THE NODAL DIAMETER OF THE MODAL PROBLEM FOR $\mu \sim o(1)$

Disk and Blade Masses Comparable

The standard case in real life is that the mass of the disk and the rotor blades is comparable ($\mu \sim o(1)$). This is true for low-pressure turbines and compressors while high-pressure turbines tend to have much heavier disks due to shaft rotational speed and temperature effects and in the same direction compressor blades tend to have very light blades.

The dispersion relation may be written as:

$$\tilde{\omega}^4 - \left[\left(1 + \frac{1}{\mu} \right) + 4 \left(\frac{\kappa}{\mu} \right) \sin^2 \frac{\Theta}{2} \right] \tilde{\omega}^2 + 4 \left(\frac{\kappa}{\mu} \right) \sin^2 \frac{\Theta}{2} = 0 \quad (10)$$

Different expansions for the solution may be obtained for High Nodal Diameters: $\frac{n}{N} \propto \Theta \gg \kappa^{-1/2}$ or

Low Nodal Diameters: $\frac{n}{N} \ll \kappa^{-1/2}$, otherwise the dispersion relation may not be simplified.

The derivation of the expansions for the different limits are a simple exercise of regular/singular perturbations and are left to the reader as a simple exercise. The main conclusions are outlined in the following lines.

- If $4 \left(\frac{\kappa}{\mu} \right) \sin^2 \frac{\Theta}{2} = \frac{1}{\epsilon} \ll 1$ or $\kappa \Theta^2 \ll 1$, the low nodal diameter region which is dominated by the disk dynamic is obtained. The dispersion relation reduces to:

$$\tilde{\omega}^4 - \left(1 + \frac{1}{\mu} \right) \tilde{\omega}^2 = 0 \quad (11)$$

and hence the natural frequency of the disk in zero in first approximation, $\tilde{\omega}_{Disk}^2 = 0$, and the natural frequency of blade dominated modes experience a correction due to the Disk mass, $\tilde{\omega}_{Blade}^2 = \left(1 + \frac{1}{\mu} \right)$.

The governing equations for nodal diameters satisfying the condition $n/N \ll \kappa^{-1/2}$ are:

$$\begin{aligned} \mu \frac{d^2 x_j}{d\tau^2} &= (y_j - x_j) \quad \frac{d^2(\mu x_j + y_j)}{d\tau^2} = 0 \\ &\text{or} \\ \frac{d^2 y_j}{d\tau^2} &= -(y_j - x_j) \quad \mu \frac{d^2(x_j - y_j)}{d\tau^2} = (1 + \mu)(y_j - x_j) \end{aligned} \quad (12)$$

- The 1st equation represents a rigid body motion of the center of mass of the sector ($\omega_{Disk}^2 = 0$) of the sector.

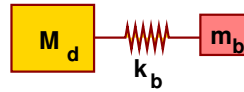


Figure 14: DYNAMIC MODEL REPRESENTATIVE OF A BLADE-DISK LOW NODAL DIAMETER MOTION

- The 2nd equation is an harmonic motion with a natural frequency of $\omega^2 = \frac{1+\mu}{\mu}$. The blade and the disk move in anti-phase while the center of mass of the assembly is fixed. The equivalent system is the following:

Everything happens as if the disk sectors were uncoupled among them and the rotor blade and the disk were joined through a spring of stiffness k_b .

- If $4 \left(\frac{\kappa}{\mu} \right) \sin^2 \frac{\Theta}{2} = \frac{1}{\epsilon} \gg 1$, or $\kappa \Theta^2 \gg 1$, the high nodal diameter limit of the problem is obtained. The dispersion relation reduces in this case to:

$$\epsilon \tilde{\omega}^4 - \tilde{\omega}^2 + 1 = 0$$

and hence $\tilde{\omega}_{Disk}^2 = \frac{1}{\epsilon}$ and $\tilde{\omega}_{Blade}^2 = 1$. The natural frequency of the rotor blade dominated modes is the same a similar to that of the blade alone case

- if $\epsilon \sim 1$, or $n/N \sim \kappa^{-\frac{1}{2}}$, no simplification is possible

3 Unsteady Aerodynamics

Introduction

Unsteady aerodynamics associated to vibrating airfoils is complex and little can be said with a large degree of generality. Computational methods based on the solution of the linearized Navier-Stokes equations are widely used in the gas turbine industry, and even fully non-linear unsteady methods are used for some specific problems. The accuracy of computational method is acceptable for most of the cases, especially within the industry where codes have been tuned for specific flows, however the physical understanding of these flows is reduced.

Unsteady pressure distributions have little to do with steady pressure fields and the variability is even larger. To begin with the base mean flow has a strong influence in the perturbations. Steady aerodynamics of low-pressure turbines which is a high subsonic Mach number flow subject to a large turning, has little to do with compressor aerodynamics that may even change dramatically from operating point to operating point. Compressor flows have low turning but may include shock waves at different positions. Moreover new parameters such as the reduced frequency, or Strouhal number, the phasing between the vibration of neighbouring airfoils or the mode-shapes themselves appear, making the variability of the problem very large. On the top of that the unsteady pressure itself is not the main interest of the aerolastic analyst, but the aerodynamic damping, that depends completely on the phasing between the unsteady pressure and the blade surface. For all these reasons and general view of the unsteady aerodynamics of vibrating airfoils in turbomachinery is not available.

Large modulus of unsteady pressure may be seen in high velocity regions, such as the pressure side of turbines and high gradient regions, such as the vicinity of shock waves (see Fig. 15).

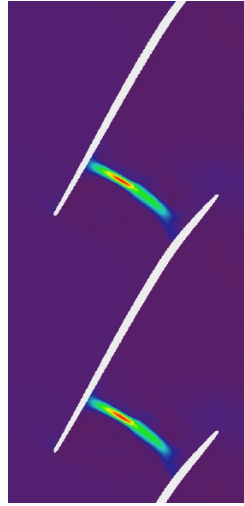


Figure 15: UNSTEADY PRESSURE OF A TRANSONIC COMPRESSOR VIBRATING IN FLAP MODE.

Unsteady Aerodynamics of Vibrating Airfoils

The order of magnitude of the modulus of unsteady pressure of a vibrating airfoil with amplitude δ_{max} and angular frequency ω , may be estimated using the momentum equation of an inviscid flow

$$\rho \frac{D\mathbf{v}}{Dt} = -\nabla p \quad (13)$$

If we assume that the flow may be decomposed in a mean flow where $\mathbf{v} = \mathbf{v}_0(\mathbf{x}) + \mathbf{v}'(\mathbf{x}, t)$, $p = p_0(\mathbf{x}) + p'(\mathbf{x}, t)$ where the sub-index 0 denotes mean flow and the prime the unsteady perturbed variables. The order of magnitude of the unsteady perturbation, Δp_c , may be estimated as

$$\Delta p_c \sim \rho U_c \omega \delta_{max} \max(1, k) \quad (14)$$

where the reduced frequency, k , or the Strouhal number, St , is defined as $k = \omega c / U_c$, where c , is the chord or the characteristic length and U_c is a characteristic velocity. For flutter cases the reduced frequency is of order unity, typically $k < 1$ and therefore in practice

$$\Delta p_c \sim \rho U_c \omega \delta_{max}. \quad (15)$$

The unsteady force in the airfoil is then

$$F^a \sim \rho U_c \omega \delta_{max} S = F_c \quad (16)$$

where S is the airfoil surface. The unsteady forced in the j^{th} -airfoil may be expressed as:

$$F_j^a = F_c \tilde{F}(k, \sigma, t). \quad (17)$$

The inter-blade phase angle (IBPA) σ is the phase difference between two adjacent airfoils and is directly related with the nodal diameter. Figure 16 sketches the vibration of a compressor airfoil with $\sigma = 90^\circ$. The minimum flow unit needed to represent this vibration is four passages. Airfoils 2 and 4 have reached its maximum deflection and vibrate in anti-phase while airfoils 1 and 3 are passing through its zero deflection position but with opposite velocities. Nodal diameter $ND = N_b/2$ corresponds with $\sigma = 180^\circ$ and has

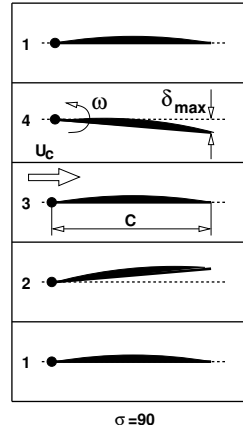


Figure 16: INTER-BLADE PHASE ANGLE INTERPRETATION

the shorter wave-length corresponding to two passages, while $ND = 1$ corresponds to $\sigma = 2\pi/N_b$ and would involved the simulation of the whole wheel.

The most distinctive feature of the unsteady aerodynamics of vibrating airfoils in turbomachinery is that the unsteady force in the j^{th} -airfoil depends on the motion of all the airfoils,

$$F_j^a = F_c \tilde{F}_j(k, x_1, x_2, \dots, x_j, \dots, x_N, t) \quad (18)$$

In the particular case that the airfoils motion is harmonic in time, $x_j = \hat{x}_\omega e^{i\omega t}$ and that all the airfoils move with a common inter-blade phase angle, $x_j = \hat{x}_n e^{in x_j}$, then the force in the airfoil j , may be expressed as a summation of the contribution of the different temporal and spatial harmonics

$$F_j^a = \text{Re}(F_c \sum_{\omega} \sum_n \hat{F}_{n,\omega}(\mathbf{x}) e^{i(n x_j + \omega t)}) \quad (19)$$

Moreover, if the unsteady perturbations are much smaller than the mean flow, $p'(\mathbf{x}, t) \ll p(\mathbf{x})$, the unsteady aerodynamics is linear. A necessary condition is then that

$$\frac{\Delta p_c}{p_c} \sim \frac{\rho_c U_c \omega \delta_{Max}}{p_c} \sim M^2 St \frac{\delta_{Max}}{c} \quad (20)$$

that always can be achieved if the blade displacements are small enough, $\delta_{Max}/c \ll 1$ and typically $\delta_{Max}/c \sim 10^{-2}$. In this case the solution is harmonic in time, i.e.: composed in first in first approximation of a single harmonic corresponding with the vibration frequency. The contribution of higher harmonics is negligible since are the results of non-linear interactions,

$$F_j^a = \text{Re}(F_c \sum_n \hat{F}_n e^{i(n x_j + \omega t)}) \quad (21)$$

The unsteady pressure, or any perturbation variable, are also proportional to the vibration amplitude and therefore it is interesting to scale the blade force with δ_{Max}

$$F_j^a = \text{Re}(F_c / \delta_{max} \sum_n \hat{f}_n(\omega) \hat{x}_n e^{i(n x_j + \omega t)}) \quad (22)$$

It is interesting to note that the unsteady force Fourier coefficients, \hat{f}_n , depend on the non-dimensional angular frequency and the inter-blade phase angle, $\hat{f}_n(k = \omega c / U_c, \sigma)$ and are complex numbers since aerodynamics effects translates in an apparent stiffness (Real part) and damping (Imaginary part)

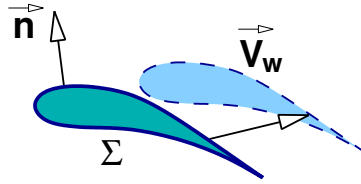


Figure 17: MOVING SURFACE OF A VIBRATING AIRFOIL

Aerodynamic Work-per-Cycle

Relationship with Aerodynamic Coefficients The work-per-cycle performed by the aerodynamic forces is

$$W_{aero} = \int_0^T \left(\int_{\Sigma} p(x,t) \mathbf{V}_w \cdot \mathbf{n} dA \right) dt \quad (23)$$

If we assume that there is no spatial dependency of the pressure to simplify the formulation, i.e.: $p = p(t)$, and the same is true for the airfoil motion, $\mathbf{V}_w = \mathbf{V}_w(t)$, then

$$\int_{\Sigma} p(x,t) \mathbf{V}_w(x,t) \cdot \mathbf{n} dA = \mathbf{V}_w \cdot \int_{\Sigma} p(t) \mathbf{n} dA = \mathbf{V}_w \cdot \mathbf{F}(t) \quad (24)$$

and we seek harmonic solutions $\mathbf{x}_w = \hat{\mathbf{x}} e^{i\omega t} \Rightarrow \mathbf{V}_w(x,t) = i\omega \hat{\mathbf{x}}_w e^{i\omega t}$ and $\mathbf{F} = \hat{\mathbf{F}} e^{i\omega t}$ then the work per cycle is $W_{work-per-cycle} = \pi(\hat{F}_I \hat{x}_R - \hat{F}_R \hat{x}_I)$. If we set the time origin such as $x = \hat{x}_R \cos \omega t$, (i.e.: $\hat{x}_I = 0$), then

$$W_{work-per-cycle} = \pi \hat{F}_I \hat{x}_R \quad (25)$$

This means that the damping is associated to the imaginary part of the forced coefficient. In the general case that the pressure and the mode-shape are a function of the position the same result may be obtained if the order of the spatial and temporal integral is exchanged.

Non-Dimensional Aerodynamic Work Aerodynamic work-per-cycle, W_{aero} , may be scaled from a pure aerodynamic point of view using the unsteady pressure estimate (Eq. 15) as

$$\Theta = \frac{W_{aero}}{2\pi\rho U_c \omega \delta^2 S} \quad (26)$$

This non-dimensionalization absorbs the quadratic dependency with the amplitude that is obtained for linear aerodynamics. Non-dimensional aerodynamic work, Θ , depends on the following parameters

$$\Theta = \Theta \left(\underbrace{k}_{\text{Freq.}}, \underbrace{\text{Mode-shape}}_{\text{IBPA+Family}}, \underbrace{\frac{\delta}{c}}_{\text{Non-Linear}}, \underbrace{M, Re, \alpha_{in}}_{\text{Steady-Field}} \right) \quad (27)$$

Reduced frequency, k , is usually used as a target design criterion to fix flutter problems, both in the conceptual and in the detailed design phase. Natural frequencies are raised either increasing the blade chord, the thickness or both. The most powerful mechanism of controlling the reduced frequency is the blade aspect ratio.

However aerodynamic damping sensitivity with the mode-shape is much larger. Damping change strongly with the inter-blade phase angle, σ , but even focusing in the most critical σ , the position of the centre of torsion of the airfoil may dramatically change the aerodynamic damping. The most clear example is the

change in aerodynamic damping between flap and torsion modes. The center of torsion location must be carefully controlled to drive the designs in the right direction.

Aerodynamic damping is in general insensitive to the vibration amplitude except in particular non-linear problems, such as shock flutter, where the aerodynamic damping may even change of sign with the vibration amplitude.

Steady aerodynamics flow-field obviously change the aerodynamic damping and is responsible of the completely different behaviour of compressor and turbines, but for a given application the variability with the Mach number for instance is reduced since this is fixed by purely aerodynamic criteria and it is not a free parameter. Sensitivity of the aerodynamic damping to the Reynolds number is small, since the unsteady pressure caused by the airfoil motion are mainly an inviscid phenomenon. Perhaps the only exception would be compressor stall flutter where separation is controlled by viscous effects. Incidence change caused by shaft speed variation may heavily change the flow-field and hence the aerodynamic damping, especially in compressors.

Aerodynamic damping may be also scaled assuming that it will take part of the airfoil motion equations, that for a single degree of freedom systems take the form:

$$m\ddot{x} + c\dot{x} + kx = 0 \quad (28)$$

that may be non-dimensionalised using $\tau = \omega_n t$ and $\dot{x} = x'\omega_n$ to obtain

$$x'' + 2\xi x' + x = 0 \quad (29)$$

where the **Critical Damping Ratio**, ξ , is defined as $\xi = c/2m\omega_n$. Viscous damping, c , is related with the aerodynamic forces as $c = \frac{1}{\omega_n} \text{Im}(\hat{F}_a/\hat{x}_R)$, where \hat{x}_R is the real part of the displacement that in practice may be translated as the maximum displacement of the airfoil, $\hat{x}_R = \delta_{max}$. Taking into account that the imaginary part of the aerodynamic force and the aerodynamic work are related by $\hat{F}_a = W_{aero}/\hat{x}_R$, the critical damping ratio reduces to

$$\xi = \frac{1}{m\omega_n^2} \frac{W_{aero}}{2\pi\delta_{max}^2} \quad (30)$$

which is nothing else that another form of non-dimensionalizing the aerodynamic work. The aerodynamics work is usually obtained from an unsteady aerodynamic simulation while m , here is the modal mass. Critical damping ratio and non-dimensional work are related by the expression

$$\xi = \Theta\rho U_c S/m\omega_n = \mu\Theta/k \quad (31)$$

where $\mu = \rho c S/m$ which is a measure of the ratio between the mass of the air surrounding the airfoil and the mass of the blade, $\mu \sim m_{air}/m_{blade}$. It must be noticed that a change of the blade material density may change the critical damping ratio while leaving unaffected the non-dimensional aerodynamic work-per-cycle which is a purely aerodynamic quantity.

Reduced Frequency and Mode-Shape Effects in Turbines

It has already been mentioned that to increase the reduced frequency is the most standar mechanisms to stabilise unstable configurations. To illustriate this phenomenon we have chosen a state of the art low-pressure turbine aifoil.

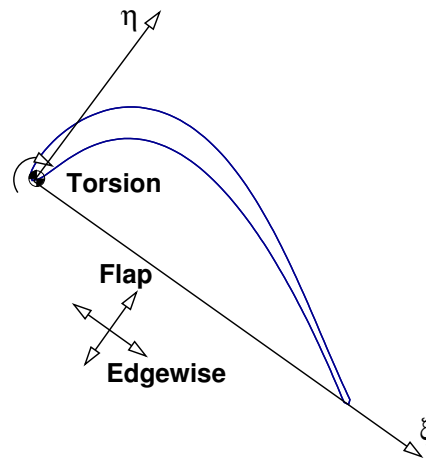


Figure 18: DESCRIPTION OF FUNDAMENTAL MODE-SHAPES

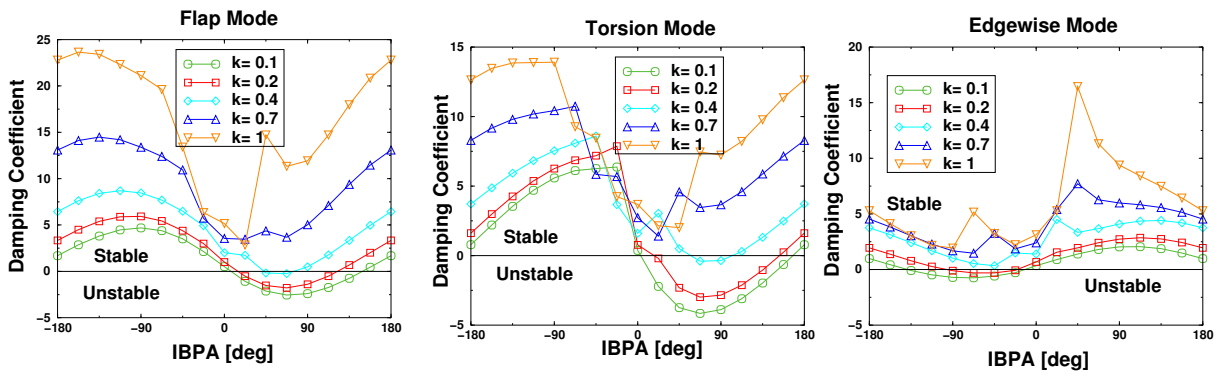


Figure 19: DAMPING COEFFICIENT AS A FUNCTION OF IBFA AND REDUCED FREQUENCY FOR THE FLAP (LEFT), TORSION (MIDDLE) AND EDGE-WISE (RIGHT) MODES.

The fundamental modeshapes are described in Fig. 18. The edgewise and flap modes are defined as bending modes along and perpendicular to the chord. The centre of torsion of the third fundamental mode is located at the l.e. of the airfoil. The airfoil used in all the simulations corresponds to the mid-section of a representative rotor blade ($\alpha_{inlet} = 37^\circ$, $\alpha_{exit} = 64^\circ$, $M_{is} = 0.76$ $Re = 2.5 \times 10^5$). Modern LPTs may have large separation bubbles on the pressure side of the airfoils that may not be accounted for using inviscid simulations. They induce phase shifts in the p.s. of the airfoil whose relative importance depends on the case. Usually, the contribution to the work per cycle of the airfoil pressure side is smaller than that of the suction side. However to avoid any further problems, all the simulations performed in the present study have retained viscous effects since its extra cost compared to the inviscid simulations is negligible.

Figure 19 shows the damping coefficient as a function of the IBPA for the different fundamental modes previously described. In general the IBPA may be defined as $\sigma = 2\pi(m-1)/N_s$ where $m = 1 \dots N_s$ and N_s is the number of sectors. For a freestanding airfoil $N_s = N_{blades}$. The stabilizing effect of the reduced frequency can be seen for all the modes but there is always a region of unstable IBPA for the computed range of reduced frequencies. Torsion modes are the most unstable ones, this is a quite general trend, but all the modes may become unstable if the reduced frequency is low enough. More details may be found in [3].

For low reduced frequencies non-dimensional work-per-cycle has a sine-like dependency with the inter-blade phase-angle. This is a clear indication that the destabilizing effect is due to the presence of immediately adjacent airfoils. The damping curves show as well some spikes superimpose to the sine-like curves that are due to acoustic resonances at the inlet and outlet of the airfoil and that show-up in the simulations. The IBPA at which the resonances occurs increases with the reduced frequency. It is clear

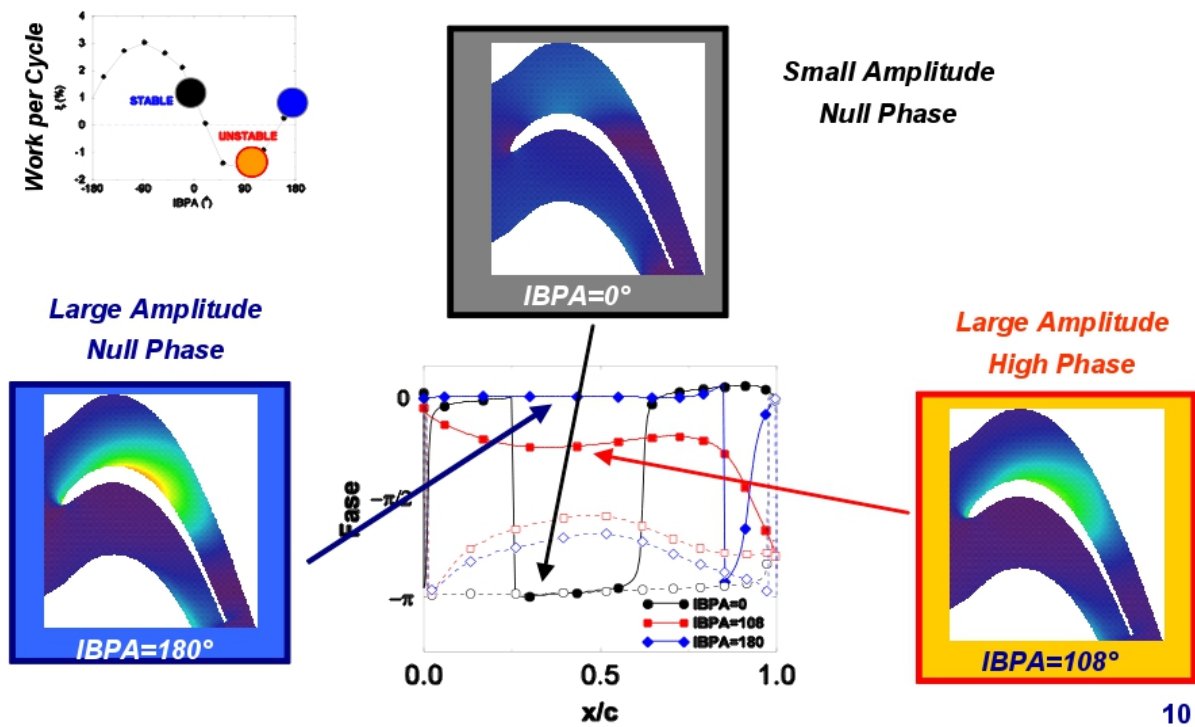


Figure 20: PHYSICS OF A LOW-PRESSURE TURBINE AERODAMPING

that for high enough reduced frequency all the modes may be stabilized being the frequency at which this happens mode dependent.

Figure 20 summarises well understood unsteady effects of a single low-pressure turbine airfoil at relatively low reduced frequencies ($k \simeq 0.2$) for a torsion about the l.e. mode.

The simulations of the fundamental modes for a single airfoil indicate that, the most unstable IBPA is around $\pm 90^\circ$, depending on the mode, while the $\sigma = 0^\circ$ and $\sigma = 180^\circ$ are only slightly damped. This behaviour may be readily understood by noting that the modulus of the unsteady pressure for the $\sigma = 0^\circ$ case is much smaller than for the $\sigma = 180^\circ$ case. This is sketched in Fig. 20 where the modulus of the unsteady pressure generated by the airfoil vibrating in torsion about the leading edge for $\sigma = 0^\circ$, $\sigma = 90^\circ$ and $\sigma = 180^\circ$ are displayed. It is clearly seen that the modulus of the unsteady pressure is very small for $\sigma = 0^\circ$ since the relative displacement between the two airfoils in the throat region is very small compared to the one that is obtained for $\sigma = 180^\circ$, where both airfoils move in anti-phase. For an $\sigma = 90^\circ$ the modulus of the unsteady pressure lies in between the other two.

Since the work per cycle depends strongly on the phase between the unsteady pressure and the blade displacement this aspect is reviewed in the following lines. Figure 20 (middle) displays the unsteady pressure phase for the $\sigma = 0^\circ$, $\sigma = 90^\circ$ and $\sigma = 180^\circ$. It is important to recall that the unsteady pressure on the suction side (filled symbols) is significantly larger than the one on the pressure side (open symbols). Therefore, only the phase of the former will be discussed. The phase of $\sigma = 0^\circ$, and $\sigma = 180^\circ$ is zero in first approximation. This means that, both modes are neutral from a stability point of view. When the blade moves closing the throat, the pressure is increased in that region, tending to damp the vibration in that part of the cycle but that energy is transmitted back to the airfoil in the second part of the cycle. The damping for $\sigma = 180^\circ$ is dominated by the pressure side which is the only region with a non-null phase with the airfoil. The most critical IBPAs are those in which the modulus of the unsteady pressure is high and the pressure raise when the airfoil moves opening the throat (i.e. when the motion of the suction-side neighboring airfoil closing the throat leads the motion of the reference airfoil)

Two different concepts are used in the industry to mitigate flutter in turbines. The most standard and widespread solution is the use of interlock rotors where the rotor blade shrouds are let to get in contact

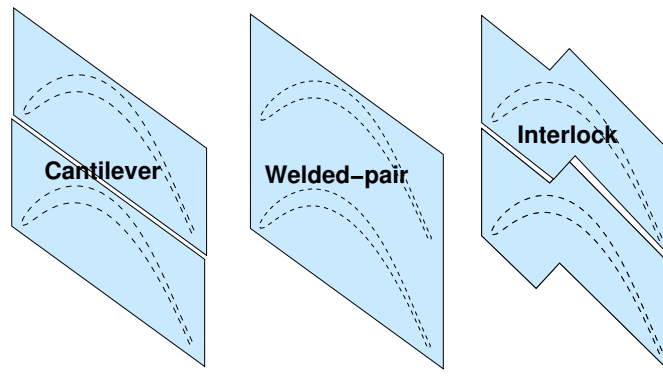


Figure 21: DIFFERENT SOLUTIONS ADOPTED TO MITIGATE FLUTTER ON TURBINE AIRFOILS

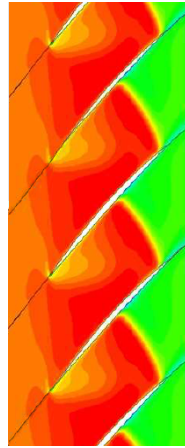


Figure 22: MACH NUMBER FLOW-FIELD OF A CHOKED COMPRESSOR

to increase the frequency of the assembly, especially for high NDs, and modify the mode-shapes. Se second solution, adopted whenever possible in the RR group is the used of welded-in-pair rotor blades, that do not increase significantly the natural frequencies of the bladed-disk but increase dubstantially the aerodynamics damping (see Figure 21)

Compressor Choke Flutter

Compressors operate in a wide range of pressure ratios and shaft speeds that give rise to quite different base flow-fields. A particular case is that in which there is a shock wave inside the compressor passage as it is depicted in figure 22. The shock-wave extends from the trailing-edge of the suction side to the compressor side. In this case the instability is caused by the shock wave oscillation between neighbouring airfoils caused by the airfoil vibration that modifies the throat area. The instability occurs at large reduced frequencies ($k \gg 0.3 - 0.4$) and the sensitivity to this parameter is low. Choke flutter is less common than other types of compressor flutter and it is usually experienced by middle and rear compressor stages.

The numerical prediction of the instability is difficult (**author?**) [4] since this is the result of the compensation of two large quantities as it is sketched in figure 23. The oscillation of the shock-wave causes large unsteady perturbations in its vecinity, both in the pressure and suction sides. The pressure side is stabilizing while the suction side is instabilizaing. The global result depends on the subtraction of both quantities.

The problem is highly non-linear since the perturbations caused by the oscillation of the shock-wave are large. In this case it has been shown that the stability of the system depends on the vibration amplitude. For small amplitudes the system may be unstable, but for large vibration amplitudes the non-linearity may lead to an stable situation as it is shown in figure

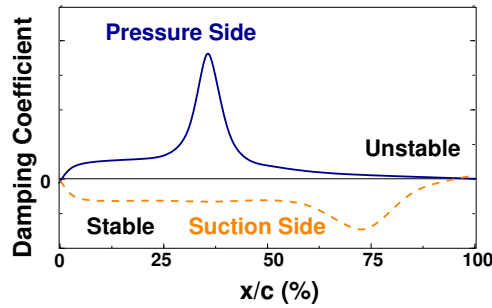


Figure 23: DAMPING COEFFICIENT DISTRIBUTION OF THE PRESSURE (SOLID LINE) AND SUCTION SIDE (DASHED LINE) OF A CHOKE COMPRESSOR.

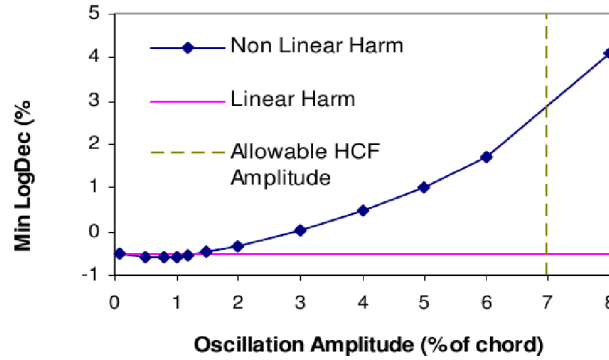


Figure 24: Stability of a choked compressor as a function of the vibration amplitude

Computation of Unsteady Forces

The Navier-Stokes equations in conservative form can be written as

$$\frac{d\mathbf{U}}{dt} = \mathbf{R}(\mathbf{U}), \quad (32)$$

where \mathbf{U} are the conservative variables. The flow may be decomposed in two parts: a steady flow and a small harmonic unsteady perturbation:

$$\mathbf{U}(\mathbf{x}, t) = \mathbf{U}_0(\mathbf{x}) + \text{Re}(\hat{\mathbf{u}}(\mathbf{x})e^{i\omega t}) \quad (33)$$

where U_0 is the background steady or mean flow and $\hat{\mathbf{u}}$ is the complex perturbation. The unsteady perturbation $\mathbf{u} \ll \mathbf{U}_0$. The background steady flow is solved using the fully non-linear steady RANS equations. The equations may be linearised about the mean flow to obtain

$$\frac{d\mathbf{u}}{dt} = \mathbf{A}(\mathbf{U}_0)\mathbf{u}. \quad (34)$$

Aerodynamic forces are usually computed in a very specific form:

1. Harmonic in time. This allows to:

- (a) Transform the Navier-Stokes equations to the Fourier space ($\mathbf{u} = \hat{\mathbf{u}}e^{i\omega t}$) to remove the time dependent character of the equations

$$i\omega\hat{\mathbf{u}} = \mathbf{A}(\mathbf{U}_0)\hat{\mathbf{u}} \quad (35)$$

- (b) Solve the resulting set of complex equations in a pseudo-time, τ , to speed-up the convergence

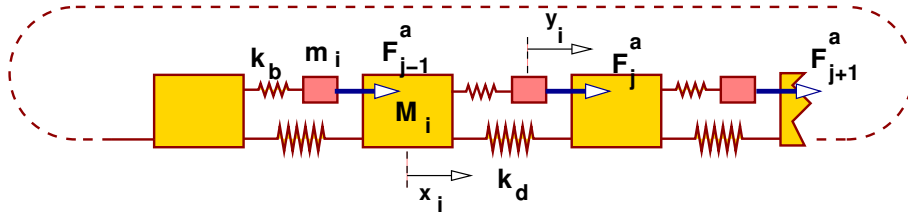


Figure 25: MASS-SPRING LUMPED MODEL INCLUDING AERODYNAMIC FORCES

of the system.

$$\frac{d\hat{\mathbf{u}}}{d\tau} + i\omega\hat{\mathbf{u}} = \mathbf{A}(\mathbf{U}_0)\hat{\mathbf{u}} \quad (36)$$

2. Travelling-Wave form, or in other words constant IBPA. This allows to reduce the computational domain to a single passage using phase shifted boundary conditions and avoid the computation of the flow-field in the whole bladed-disk wheel, significantly reducing the computational time. The phase-shifted boundary conditions in the Fourier space may be expressed as:

$$c.c.: \hat{\mathbf{u}}(\theta_0 + pitch) = \hat{\mathbf{u}}(\theta)e^{i\sigma} \quad (37)$$

where σ is the inter-blade phase-angle. The same condition may be expressed in the physical domain as $\mathbf{u}(\theta_0 + pitch, t) = \mathbf{u}(\theta, t - \Delta T)$.

The system is solved $N_\omega \times N_\sigma$ times where N_ω is the number of frequencies (family modes) to be considered, N_σ is the Number of IBPAs, if all of them are computed them $N_\sigma = 2$ NDs. This is about $10 \times$ to $100 \times$ times more efficient than solving the time-dependent non-linear equations and reaching a periodic converged state. Most if not all gas turbine manufacturers follow this approach.

4 Flutter Stability

Flutter is an aeromechanic instability and therefore requires the joined formulation of the aerodynamic and the structural problem to derive any meaningful result. Here we will first introduce the aerodynamic forces in our simplified lumped model and then we will generalised the formulation to arbitrary bladed-disks.

Aeroelastic Lumped Model

The basic lumped model that we have used in previous sections may be extended to include the aerodynamic forces due to the motion of the arfoil itself. The governing equations of the disk are not modified

$$M_{Disk} \frac{d^2 x_j}{dt^2} = k_{disc}(x_{j+1} - x_j) - k_{disc}(x_j - x_{j-1}) + k_{blade}(y_j - x_j) \quad (38)$$

but the rotor blade equation have to include the motion dependent aerodynamic forces, F_j^a ,

$$m_b \frac{d^2 y_j}{dt^2} = -k_{blade}(y_j - x_j) + F_j^a(x_1, x_2, \dots, x_N, \omega) \quad (39)$$

The most distinctive characteristics of the aerodynamic forces is that they couple the motion of all the blades while the coupling through the disk elastic forces just couples the neighbouring sector, i.e.: sector j is only coupled with sectors $j \pm 1$. Obviously the aerodynamic influence of near-by airfoils is greater than that that are far apart, but conceptually all the blades are coupled through the aerodynamics. Even

if the disk is infinitely stiff and we decouple the blades from the disk assuming that $x_j = 0$ for all j resulting in a set of N independent equations, the aerodynamics recouples all the blades because the the motion of the airfoil j influence the rest of the blades. The non-dimensional form of the equation is:

$$\begin{aligned}\mu \frac{d^2 x_j}{d\tau^2} &= \kappa(x_{j+1} - 2x_j + x_{j-1}) + (y_j - x_j) \\ \frac{d^2 y_j}{d\tau^2} &= -(y_j - x_j) + \tilde{F}^a(x_1, \dots, x_N)\end{aligned}\tag{40}$$

where $\mu = \frac{M}{m}$, $\kappa = \frac{k_{disk}}{k_{blade}}$, $\tau = \frac{t}{t_c}$, $t_c = \sqrt{\frac{m}{k_{blade}}} = \omega_a^{-1}$ as it has been mentioned before. Aerodynamics is a **small correction** of the structural problem. Non-dimensional forces, $\tilde{F}^a = F^a/m\omega_a^2$, are of the order of the critical damping ratio, ξ , typically around 10^{-2} .

To further progress in the understanding of the flutter problem is essential to first understand how the aerodynamic forces interact with the structure, and how they are computed. This is better seen recurring to a more generic formulation that eventually could be applied to any bladed-disk.

Formulation of the Tuned Flutter Problem

The equations of motion for the small amplitude vibration of a perfectly tuned bladed disk with N identical sectors, in the absence of any external forcing except for the linear aerodynamic effects, take the form

$$\mathbf{M}\ddot{\mathbf{x}} + \mathbf{K}\mathbf{x} = \mathbf{L}(\mathbf{x})_{\text{aero}},\tag{41}$$

where the bladed disk degrees of freedom (after an appropriate FEM discretization) are stored in $\mathbf{x}(t)$, \mathbf{M} and \mathbf{K} are the mass and stiffness matrices, both symmetric and positive definite, and \mathbf{L}_{aero} accounts for the aerodynamic forces. Structural damping has been neglected; the only source of damping considered in the formulation above is that coming from the aerodynamic terms, which is typically the dominating one for low reduced frequencies, see e.g. [?].

The vibration modes of the system can be written using complex notation as

$$\mathbf{x} = \mathbf{X}e^{i\omega t} + \text{c.c.},\tag{42}$$

where the vibration mode shape \mathbf{X} and the mode oscillation frequency and damping ω (c.c. stands for the complex conjugate) are given by the following eigenvalue problem

$$(\mathbf{K} - \omega^2 \mathbf{M})\mathbf{X} = \mathbf{M}_{\text{aero}}(\omega)\mathbf{X},\tag{43}$$

which requires the knowledge of the matrix of aerodynamic forces \mathbf{M}_{aero} as a function of ω . The calculation of \mathbf{M}_{aero} for a given ω value involves the solution of the linearized Navier-Stokes equations that prescribe the airflow around the blades for all linearly independent blade displacements. Therefore, the computation of the bladed disk vibration characteristics using the fully coupled structural-aerodynamic formulation given by Eqn. (43) is extremely costly and simply not realizable for any realistic configuration of practical interest.

The computational cost of this problem is drastically reduced if one takes into account the fact that the aerodynamic effects produce only small variations of the purely structural vibration frequencies. With this idea in mind, we will first rewrite Eqn. (43) using the structural mode basis and then apply an asymptotic perturbation method to obtain the first order aerodynamic correction of the purely structural vibration characteristics. This is a well known procedure to compute the aerodynamic stability properties

of tuned bladed disks (see [? ?] for a recent application of this approach in two and three dimensional configurations).

Structural vibration modes.

If the response vector (42) is partitioned as

$$\mathbf{X} = \begin{bmatrix} X_1 \\ X_2 \\ \vdots \\ X_N \end{bmatrix}, \quad (44)$$

with the vector X_j containing the displacements of the m degrees of freedom associated with sector j , then the problem that gives the natural oscillations of the tuned bladed disk without aerodynamic effects (Eqn. (43) with $\mathbf{M}_{\text{aero}} = 0$) takes the form

$$\left(\begin{bmatrix} K & K_c & 0 & \cdots & K_c^T \\ K_c^T & K & K_c & \cdots & 0 \\ & & \ddots & \ddots & \\ K_c & 0 & \cdots & K_c^T & K \end{bmatrix} - \omega^2 \begin{bmatrix} M & M_c & 0 & \cdots & M_c^T \\ M_c^T & M & M_c & \cdots & 0 \\ & & \ddots & \ddots & \\ M_c & 0 & \cdots & M_c^T & M \end{bmatrix} \right) \begin{bmatrix} X_1 \\ X_2 \\ \vdots \\ X_N \end{bmatrix} = \begin{bmatrix} 0 \\ 0 \\ \vdots \\ 0 \end{bmatrix}, \quad (45)$$

where the $m \times m$ sector stiffness and mass matrices K and M are symmetric and the coupling between adjacent sectors is represented by the coupling stiffness and mass matrices K_c and M_c . In our model problem the mass coupling matrix is $M_c = 0$ and the number of DOF of the sector is $m = 2$.

The cyclic symmetry of the bladed disk (that is composed of a sector repeated N times and arranged periodically) is now evident in the matrices in Eqn. (45) that exhibit a block circulant structure, i.e., each row can be obtained from the previous one after a wrap-around forward block shift. The associated complex eigenvectors

$$\begin{bmatrix} X_1 \\ \vdots \\ X_j \\ \vdots \\ X_N \end{bmatrix} = \begin{bmatrix} Z_k e^{i(\frac{2\pi k}{N})1} \\ \vdots \\ Z_k e^{i(\frac{2\pi k}{N})j} \\ \vdots \\ Z_k e^{i(\frac{2\pi k}{N})N} \end{bmatrix}, \quad \text{for } k = 1 \dots N, \quad (46)$$

correspond to travelling waves with k nodal diameters that, taking into account Eqn. (42), rotate around the annulus with constant angular velocity $\frac{\omega}{(2\pi k/N)}$. The complex vector Z_k of size m contains the mode shape details and the only eigenvector variation from sector to sector is just a phase increment of amount $\frac{2\pi k}{N}$ (the so-called ‘‘interblade phase angle’’). The vector Z_k can be regarded as the k -th mode of the discrete Fourier transform of the N -periodic sequence of the sector degrees of freedom along the complete structure, X_1, \dots, X_N ; recall that the relation between Fourier modes F_1, \dots, F_N and sector degrees of freedom S_1, \dots, S_N is given by

$$S_j = \sum_{k=1}^N F_k e^{i(\frac{2\pi k}{N})j}, \quad \text{for } j = 1 \dots N, \quad \text{and} \quad (47)$$

$$F_k = \frac{1}{N} \sum_{j=1}^N S_j e^{-i(\frac{2\pi j}{N})k}, \quad \text{for } k = 1 \dots N. \quad (48)$$

Note also that it is enough to consider the value of k modulo N ; the change $k \rightarrow k + N$, that corresponds to the addition of a complete turn around the rotor, leaves all the above expressions unchanged. This effectively means that the structure is symmetric and does not distinguish between forward and backward

travelling-waves.

If we now insert expression (46) into Eqn. (45), N decoupled eigenvalue problems of size m are obtained

$$\begin{aligned} ((K_c - \omega^2 M_c) e^{i(\frac{2\pi k}{N})} + (K_c - \omega^2 M_c)^T e^{-i(\frac{2\pi k}{N})} + K - \omega^2 M) Z_k = 0, \\ \text{for } k = 1 \dots N, \end{aligned} \quad (49)$$

which, for each k , have m real eigenvalues, $\omega_{k1}^2, \dots, \omega_{km}^2 \geq 0$, that give the oscillation frequencies of the structure. The associated eigenvectors, Z_{k1}, \dots, Z_{km} , are, in general, complex. Notice that the cyclic symmetry allows to drastically reduce the computational effort required to obtain the vibration modes of the tuned bladed disk: from $\mathcal{O}(N^3 m^3)$ for solving Eqn. (45) to only $\mathcal{O}(Nm^3)$ for the N eigenvalue problems in Eqn. (46).

The eigenvalue equation Eqn. (49) remains invariant under the changes

$$k \rightarrow N - k, \quad \omega_k^2 \rightarrow \omega_{N-k}^2 \quad \text{and} \quad Z_k \rightarrow \bar{Z}_{N-k}, \quad (50)$$

and thus, for every travelling wave rotating in one direction, there is also another identical one that rotates in the opposite direction with the same velocity. This symmetry comes from the fact that the original system (41) remains unchanged after time is reversed, $t \rightarrow -t$, because it does not exhibit any dissipation at all. Travelling wave modes come thus in counter-propagating pairs, except for those associated with $k = 0$ and $k = \frac{N}{2}$ (present only for $N = \hat{2}$), which have real Z_k and can be seen as non propagative standing waves. Property (50) implies that the plot of the natural frequencies versus the number of nodal diameters, k , is symmetric, and only its first half (interblade phase angle from 0 to π) is normally plotted.

Aerodynamic correction.

In order to evaluate the aerodynamic correction of the vibration characteristics of the bladed disk it is convenient to first perform in Eqn. (43) the following change of variables to a purely structural travelling wave basis

$$\mathbf{X} = \mathbf{P}\mathbf{A}, \quad (51)$$

with

$$\mathbf{P} = \frac{1}{\sqrt{N}} \begin{bmatrix} P_1 e^{i(\frac{2\pi 1}{N})1} & \dots & P_N e^{i(\frac{2\pi N}{N})1} \\ \vdots & & \vdots \\ P_1 e^{i(\frac{2\pi 1}{N})j} & \dots & P_N e^{i(\frac{2\pi N}{N})j} \\ \vdots & & \vdots \\ P_1 e^{i(\frac{2\pi 1}{N})N} & \dots & P_N e^{i(\frac{2\pi N}{N})N} \end{bmatrix} \quad \text{and} \quad \mathbf{A} = \begin{bmatrix} A_1 \\ \vdots \\ A_j \\ \vdots \\ A_N \end{bmatrix}, \quad (52)$$

and where the vectors $A_j = [A_{j1}, \dots, A_{jm}]^T$ contain the amplitudes of the different travelling wave modes. The eigenvalue problem in Eqn. (43) takes now the form

$$\begin{bmatrix} \Omega_1^2 - \omega^2 I & \dots & 0 \\ \vdots & \ddots & \vdots \\ 0 & \dots & \Omega_N^2 - \omega^2 I \end{bmatrix} \begin{bmatrix} A_1 \\ \vdots \\ A_N \end{bmatrix} = \mathbf{P}^H \mathbf{M}_{\text{aero}}(\omega) \mathbf{P} \begin{bmatrix} A_1 \\ \vdots \\ A_N \end{bmatrix}, \quad (53)$$

with diagonal mass and stiffness matrices, see Eqs. (??) and (??), and block diagonal aerodynamic matrix

$$\mathbf{P}^H \mathbf{M}_{\text{aero}}(\omega) \mathbf{P} = \begin{bmatrix} M_1(\omega) & \dots & 0 \\ \vdots & \ddots & \vdots \\ 0 & \dots & M_N(\omega) \end{bmatrix}, \quad (54)$$

as a result of the fact that the linearized aerodynamic flow problem has also cyclic symmetry and, therefore, the modes with different nodal diameters are completely independent.

The fact that pressure travelling-waves with k nodal diameters are orthogonal to travelling-waves with $j \neq k$ nodal diameters, or in physical terms, that the work of pressure travelling-wave in the displacement of another travelling-wave is null, allows the diagonalization of the aerodynamic matrix in the TW basis. This makes that TWs are the aeroelastic modes of the tuned system. This fact has deep implications in the formulation of the problem and it is one of the reasons why unsteady aerodynamics is computed using a single passage in the TW basis.

Modes with different natural frequencies are orthogonal also. This is why bladed-disk are designed to separate mode families. Mode interaction is difficult to predict and it is ultimately the instability mechanism of coalescence flutter. This problem is sometimes impossible to avoid as it happens in vane packets, where several modes with nearly de same frequency exist for the same nodal diameter enabling the possibility of interacting among them. This is a very specific topic and it will not be adressed here.

The aerodynamic terms are small and give rise to a small correction of the purely structural vibration frequencies. For a given structural frequency $\omega_{\tilde{k}\tilde{j}}$ (corresponding to the \tilde{j} -th travelling wave mode with \tilde{k} nodal diameters), its aerodynamically corrected counterpart ω is given by Eqn. (53), and it can be approximately estimated if one takes into account the following:

1. The modes with a different number of nodal diameters are decoupled and do not play any role in the correction of $\omega_{\tilde{k}\tilde{j}}$, that is,

$$A_k = 0, \quad \text{for all } k \neq \tilde{k}. \quad (55)$$

2. The $\tilde{k}\tilde{j}$ -th equation in Eqn. (53) reads

$$(\omega_{\tilde{k}\tilde{j}}^2 - \omega^2)A_{\tilde{k}\tilde{j}} = \sum_{h=1}^m [M_{\tilde{k}}(\omega)]_{jh} A_{\tilde{k}h}. \quad (56)$$

The corrected frequency ω is close to $\omega_{\tilde{k}\tilde{j}}$, but not to the other frequencies $\omega_{\tilde{k}j}$ (we are implicitly assuming here that $\omega_{\tilde{k}\tilde{j}}$ is well apart from the rest of the frequencies corresponding to the same number of nodal diameters \tilde{k}). Therefore, if $j \neq \tilde{j}$ the term $(\omega_{\tilde{k}j}^2 - \omega^2)$ in the equation above is not small, but the aerodynamic terms, $[M_{\tilde{k}}(\omega)]_{jh}$, are small and we can neglect them to obtain

$$A_{\tilde{k}j} = 0, \quad \text{for all } j \neq \tilde{j}. \quad (57)$$

In other words, the rest of the travelling wave modes with \tilde{k} nodal diameters and different frequencies do not contribute either to the correction of the $\omega_{\tilde{k}\tilde{j}}$ in first approximation.

Flutter Computational Environment

There are a number of hierarchical approaches of increasing complexity and fidelity to compute flutter. The purpose here is not to review all these approaches and discuss their limitations and implications but to give the reader a perspective of what it could be considered has been the standard practice in the industry during the last decade, but that is still in application today.

The standard approach today is to use the assumption that the aerodynamics gives rise just to a small correction of the purely structural modes. The first step then is to compute using a FEM the natural frequencies and mode-shapes of the modes suspicious to suffer from flutter and construct a modal data base. Simultaneously the base flow for the operating condition of interest is computed using a non-linear RANS solver. The structural grid containing the mode-shapes is interpolated and transferred to the

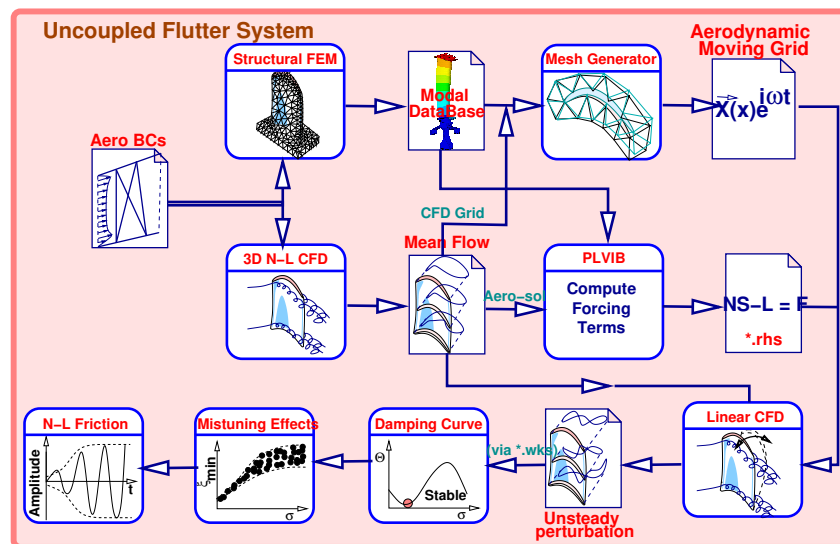


Figure 26: FLOW DIAGRAM OF A FLUTTER COMPUTATIONAL SYSTEM BASED ON A LINEAR UNCOUPLED APPROACH

aerodynamic grid and the displacements in the aerodynamic grid, due to the displacements caused by the mode-shape in the aerodynamic surface, computed. The displacements together with the base-flow solution and the natural frequency are transferred to a frequency domain linearise RANS solver. The main objective of using a linearised solver, as has been already explained, is to reduced the computational time. Moreover frequency domain solvers allow easier implementation of more accurate boundary conditions. Once the aerodynamic damping of the selected family of modes has been computed it is corrected using a reduced order model to account for mistuning. If after taking into account mistuning corrections the mode is unstable then it may be attempted to estimate the vibration amplitude of the rotor blade retaining the friction effects due to the attachments.

5 Advanced Topics

Flutter is defined as an aeroelastic instability but the problem is actually much more complex. The linear formulation of the problem just allows to predict the behaviour of the system during the early stages of the problem when the vibration amplitudes are small enough. During this phase unstable modes grow exponentially with a growth rate dictated by the aerodynamics. The exponential growth of the perturbations can not be sustained in long term and when the vibration amplitude becomes large enough non-linear terms become to play a role and the vibration amplitude saturates at a finite amplitude. The different scenarios that may take place are sketched in figure 27 (left). If the flow is stable the vibration amplitude is zero since all the modes are stable and the perturbations decay to zero. when there are unstable modes several scenario are possible. If the instability is very strong and cannot be effectively compensated by non-linear mechanisms the amplitude may become large enough to break the rotor blade. An intermediate situation is that the amplitude saturates at a finite amplitude. Then if the amplitude, and therefore the alternate stresses, is low enough the airfoil may sustain the vibration indefinitely and flutter may be acceptable since stresses caused by the limit cycle correspond to infinite life in the Goodman diagram. Alternatively if the vibration amplitude is large enough the vibration may be sustained only for a finite time and the component has finite life.

Figure 27 (middle) displays an experimental Campbell diagram of a bladed-disk undergoing flutter. High level of alternate stresses may be seen at the frequency of the unstable mode for a wide range of the shaft speed. The change in the shaft speed of the turbine implies changes both in the pressure level and the incidence. The higher in the pressure level, and hence the density, at the inlet of the turbine the higher

the vibration amplitude. In this particular cases flutter is superimposed with forced response, but only at the crossings.

When the rotor airfoils are aerodynamically unstable, the blade vibration grows up to a point in which the motion is non-linearly saturated by mechanical damping. For cantilever rotor blades this is due to the dry friction that takes place in the fir-tree attachment since they are designed to avoid the contact between neighbouring shrouds or platforms. However in principle other devices such as under-platform dampers or cover plates may contribute to increase the damping of the rotor blade. In any case what is important at this point is to estimate the vibration level of the rotor blade, that ultimately will determine the life of the component. The vibration amplitude of the airfoil is assumed to remain small enough to neglect aerodynamic non-linear effects.

The effect of friction on aerodynamically unstable rotor blades from a conceptual point of view was first studied by Sinha and Griffin [5, 6]. To clarify some of the basic issues addressed in the present investigation it is interesting to review the main results obtained from a single degree of freedom problem. If the unsteady aerodynamics is linear, then the unsteady pressure scales with the vibration amplitude, δ , and hence the aerodynamic work per cycle scales as the square of the amplitude, $W_{aero} \propto \delta^2$. The scaling of dry friction dissipation depends on the vibration amplitude. For very small vibration amplitudes ($\delta < \delta_{off-set}$) the rotor blade is stuck on the attachment and the dissipation is null, provided that the material structural dissipation is neglected. For large vibration amplitudes there is a macro displacement of the rotor blade in the attachment. The tangential force is constant and therefore the work dissipated per cycle is proportional to the displacement, $W_{macro} \propto \delta$. Between both situations there is a regime, known as micro-slip, where only a fraction of the contact surface is sliding. Different models exist to describe this behaviour (see for instance the Midlin's model [7] to describe the contact between two elastic spheres). What is important to highlight at this stage is that the work dissipated per cycle is of the form $W_{aero} \propto \delta^n$, with $n > 2$, typically $n = 3$.

The situation is sketched in Fig. When the rotor airfoils are aerodynamically unstable, the blade vibration grows up to a point in which the motion is non-linearly saturated by mechanical damping. For welded-in-pairs rotor blades this is due to the dry friction that takes place in the fir-tree attachment since they are designed to avoid the contact between neighbouring shrouds or platforms. However in principle other devices such as under-platform dampers or cover plates may contribute to increase the damping of the rotor blade. In any case what is important at this point is to estimate the vibration level of the rotor blade, that ultimately will determine the life of the component. The vibration amplitude of the airfoil is assumed to remain small enough to neglect aerodynamic non-linear effects.

The effect of friction on aerodynamically unstable rotor blades from a conceptual point of view was first studied by Sinha and Griffin [5, 6]. To clarify some of the basic issues addressed in the present investigation it is interesting to review the main results obtained from a single degree of freedom problem. If the unsteady aerodynamics is linear, then the unsteady pressure scales with the vibration amplitude, δ , and hence the aerodynamic work per cycle scales as the square of the amplitude, $W_{aero} \propto \delta^2$. The scaling of dry friction dissipation depends on the vibration amplitude. For very small vibration amplitudes ($\delta < \delta_{off-set}$) the rotor blade is stuck on the attachment and the dissipation is null, provided that the material structural dissipation is neglected. For large vibration amplitudes there is a macro displacement of the rotor blade in the attachment. The tangential force is constant and therefore the work dissipated per cycle is proportional to the displacement, $W_{macro} \propto \delta$. Between both situations there is a regime, known as micro-slip, where only a fraction of the contact surface is sliding. Different models exist to describe this behaviour (see for instance the Midlin's model [7] to describe the contact between two elastic spheres). What is important to highlight at this stage is that the work dissipated per cycle is of the form $W_{aero} \propto \delta^n$, with $n > 2$, typically $n = 3$.

The situation is sketched in Fig. 27 (right). The balance between the aerodynamic self-excitation and

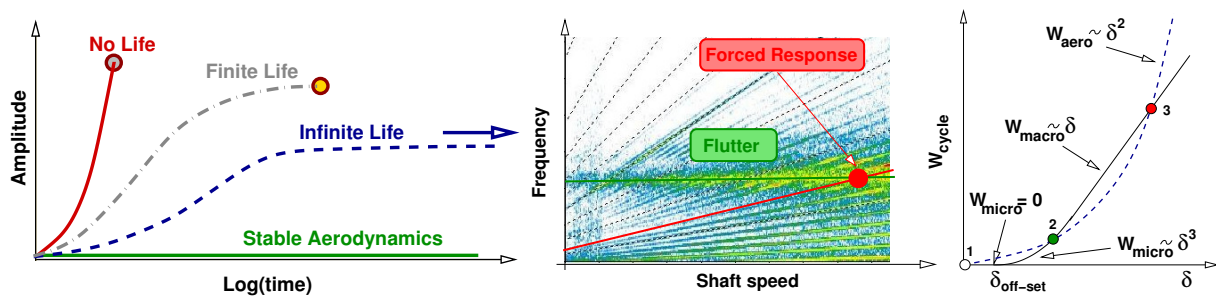


Figure 27: SUMMARY OF DIFFERENT FEATURES OF THE FLUTTER PROBLEM DURING THE NON-LINEAR SATURATED REGIME. LEFT: SCHEME OF THE POTENTIAL SITUATIONS THAT MAY BE ENCOUNTERED IN AN AERODYNAMICALLY UNSTABLE PROBLEM. LEFT: EXPERIMENTAL CAMPBELL DIAGRAM OF AN AERODYNAMICALLY UNSTABLE LP TURBINE. RIGHT: EQUILIBRIUM CHART BETWEEN THE FRICTION DISSIPATION AND AERODYNAMIC WORK.

the dry friction provides either one or three solutions, depending on the relative value between them. The trivial solution, $\delta = 0$, is unstable and any small perturbation from $\delta = 0$, moves the system towards the solution 2, which is a stable cyclic limit. Solution 2 is an attractor and any perturbation of the cyclic limit comes back to the solution 2 unless we reach the amplitude δ_3 , which is an absolute stability limit, since the solution 3 is unstable. Alternatively, if the aerodynamic self-excitation is too large, or the friction work too low, the only solution is the trivial one and the system is unstable 27 (right). The balance between the aerodynamic self-excitation and the dry friction provides either one or three solutions, depending on the relative value between them. The trivial solution, $\delta = 0$, is unstable and any small perturbation from $\delta = 0$, moves the system towards the solution 2, which is a stable cyclic limit. Solution 2 is an attractor and any perturbation of the cyclic limit comes back to the solution 2 unless we reach the amplitude δ_3 , which is an absolute stability limit, since the solution 3 is unstable. Alternatively, if the aerodynamic self-excitation is too large, or the friction work too low, the only solution is the trivial one and the system is unstable.

The consequences of flutter are quite different depending on the blade-disk configuration. Integral bladed-disks (Blisks) may only saturate aeromechanic instabilities by means of material damping that is typically of the order of 0.1% of the critical damping ratio. Cantilever blade-disks are saturated by dry friction in the contact surfaces such as fir-tree attachments and interlock contact surfaces and therefore may sustain moderate levels of instability. Saturation may be obtained as well by means of aerodynamics non-linear effects. This has been shown to happen is choke flutter [4] which is a highly non-linear problem, but in this case the saturation mechanisms are completely different.

The prediction and/or simulation of the vibration amplitude caused by the saturation by mechanical damping of aerodynamically unstable bladed-disks is quite complex and it has been addressed just by a few authors. We have used numerical methods combined with friction prediction based on scaling laws tuned with engine data to predict the vibration amplitude of unstable low-pressure turbines [8, 9]. The physics of the problem is not fully understood, especially when there are several unstable modes however it is expected that the appearance of cost effective fully-coupled non-linear methods will significantly help to understand this complex dynamic problem [10]. Although a lot of research is still needed in this area we will present here some results which are useful to understand the nature of flutter. The details may be found in [10].

A free flutter numerical experiment is considered, i.e.: there is no external periodic forcing applied in the simulation, but there are several unstable normal modes in the simulation. The main parameters of this case (aerodynamics, mass, stiffness, friction constants) have been set to reproduce a real LPT rotor; in particular, the exit Mach number is 0.57, the reduced frequency k is 0.12 and the critical damping ratio ξ for the most unstable mode is roughly 1.6% and corresponds to a flap mode in the direction of the y axis (see figure 27, left). The unsteady aerodynamic simulations consider the 2-D mid-section of the rotor;

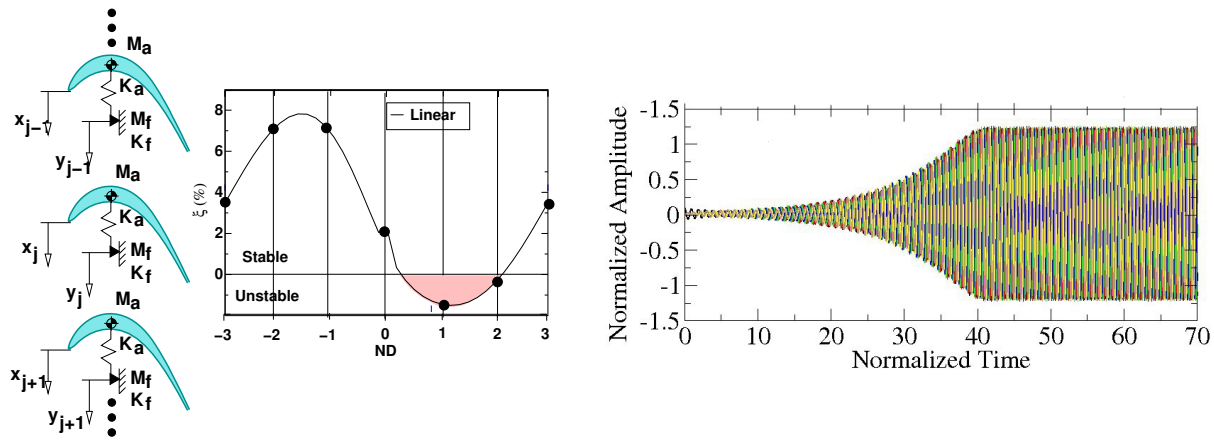


Figure 28: DESCRIPTION OF A SIMPLIFIED FULLY COUPLED NON-LINEAR AEROELASTIC MODEL. LEFT: TWO-DIMENSIONAL FLOW ABOUT A LPT AIRFOIL LINKED TO THE GROUND BY A NON-LINEAR SPRING. CENTRE: CRITICAL DAMPING RATIO OF THE LINEAR AERODYNAMICS PROBLEMS AS A FUNCTION OF THE NODAL DIAMETER. RIGHT: TIME EVOLUTION OF THE AIRFOIL DOFs.

the grid for each passage contains approximately 7000 points. Taking into account the comparatively low frequencies of the vibration, the turbulence is simulated applying the algebraic Baldwin-Lomax model with a quasi-steady approach.

The aerodynamic damping obtain using a series of linear analysis may be seen in Fig. 27, middle. It may be seen that the system is highly unstable due to the selected reduced frequency $k = 0.12$ which is very low and that several modes are unstable, the actual number depending on the number of airfoils of the configuration. A slight discontinuity may be seen around $IBPA = 0^\circ$ due to the acoustic resonances.

The first test case considers a domain with six sectors. The objective of simulating just six sectors is to observe the dynamics of a system with just two unstable modes. In this case we may see two pairs of backward and forward TWs for the $ND = 1$ and 2 plus the TWs corresponding with the ND zero and three, which are indistinguishable from the corresponding standing waves, totalizing six TWs. It may be appreciated in Fig. 29 that the forward TWs corresponding with the $ND = 1$ and 2 are unstable but with a different strength ($\xi_{ND=1}/\xi_{ND=2} \simeq 2.7$) while the rest are stable. This different growth rate of the two modes eases the derivation of conclusions and their tracking during the temporal evolution. For the initial condition of the simulation a single pair of blades is slightly displaced from its equilibrium position; this generates a perturbation in all the different TWs.

The vibration amplitudes of the airfoil DoFs using this methodology is shown in Fig. 27 (right). The time scale is normalized with the nominal vibration period of the rotor blades (i.e.: the period obtained linearizing the fir-tree constraint and neglecting aerodynamic terms), making the horizontal axis roughly equivalent to the number of vibration periods. The vibration amplitude is normalized with an analytical estimate of the maximum vibration amplitude performed using the methodology described in [9]. In practical terms the reader may think that the vibration amplitude has been normalized using the maximum *theoretical* vibration amplitude. Notice that both simulations get remarkably similar results; after an initial development stage with an exponential growth of the amplitude, the vibration saturates at a constant amplitude.

Figure 29 shows the solution post-processed using a wave-splitting method. Lines with different colours denote the evolution of different TWs. The solid lines show the evolution of the TWs using the fully coupled approach while dashed lines denote the simulation perform using the SUM approach. It may be noticed the nearly exponential growth/decay during the early stages (5-7 first periods) of the simulation; this is in good agreement with classic linear aeroelasticity theory. In table 1 The critical damping ratio for the one nodal diameter forward traveling wave, obtained from the growth rate in the first periods of

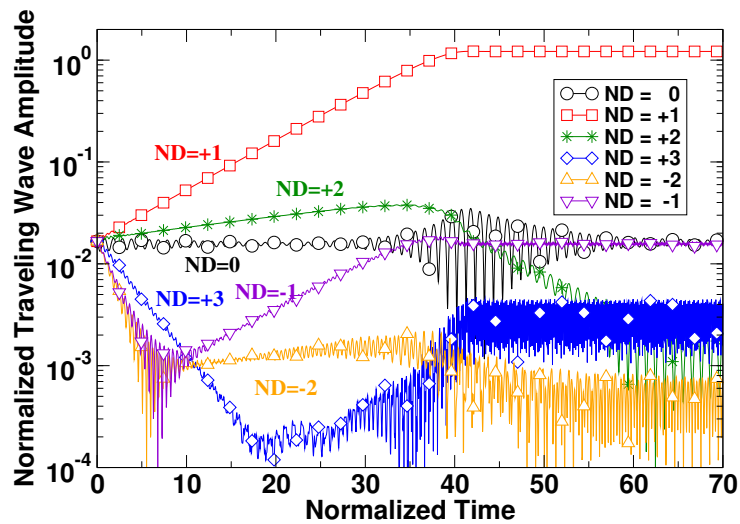


Figure 29: TIME EVOLUTION OF THE TRAVELING-WAVE AMPLITUDES IN A SIX-SECTOR COMPUTATIONAL DOMAIN

Table 1: SIX-SECTOR COMPUTATIONAL DOMAIN: CRITICAL DAMPING RATIO FOR THE MOST UNSTABLE TRAVELING WAVE

Approach	ξ
Fully Coupled	1.79%
Semi-Uncoupled	1.53%
Linear	1.56%

the simulation, can be compared with the results from a classical linear methodology. The agreement is nearly perfect for the semi-uncoupled methodology (see [10], but the differences with the fully coupled method are roughly 15%. The most unstable mode corresponds to the $ND=+1$. This is consistent with the results displayed in Fig. 29.

The behaviour of the traveling wave with nodal diameter zero (black line in Fig. 29) requires further explanation. It must be taken into account that a steady aerodynamic force (lift) with a spatial pattern corresponding to the $ND = 0$ appears in the simulation. This force was not taken into account in the determination of the initial location of the airfoils and in the long run it induces an off-set between the initial and final position of the airfoils, rather than an oscillation in the zero nodal diameter, which justifies the weird behaviour shown in the graph.

As the vibration amplitudes increase non-linear effects begin to play a greater role (10-30 periods into the simulation). In general, non linear terms allow the interaction of patterns with different nodal diameters. So, even though most waves should decay according to the linear theory, once the most unstable mode reaches a large enough vibration amplitude the system does not behave any longer linearly. Notice however that, in any case, the vibration amplitudes of the stable waves are 2-3 orders of magnitude smaller than the amplitude of the most unstable mode.

Close to the saturation (30-60 periods into the simulation) the growth rates for the unstable modes decrease. Interestingly, while the most unstable mode tends towards a constant amplitude, the energy of the other unstable mode is drained and its amplitude limited to a fairly small value. This process is still active even after the envelope of the physical amplitude of the blades has already reached saturation (about period 40). This means that there is a non-linear process that adjusts the vibration phase of the airfoils at a fairly constant vibration amplitude.

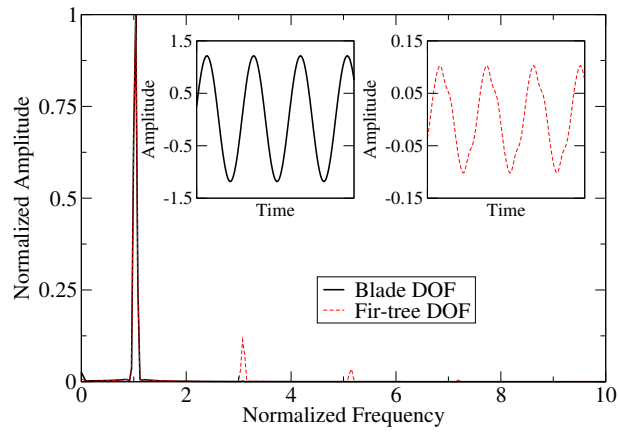


Figure 30: SIX-SECTOR MODEL: TEMPORAL HARMONIC CONTENT OF THE PERIODIC SOLUTION

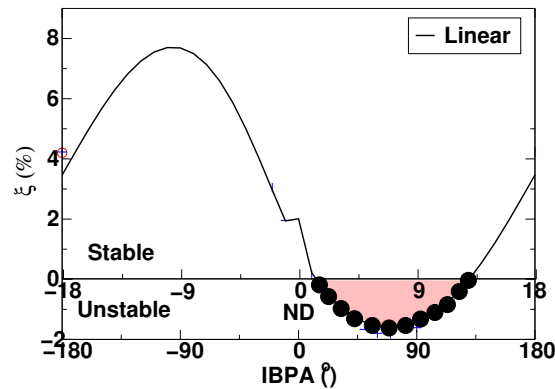


Figure 31: AERODYNAMIC DAMPING FOR THE 36-SECTOR MODEL

This conclusion is quite remarkable since although in principle it could be thought that the saturated solution could be made up of a blend of the two unstable modes, the non linearity of the fir-tree filters out the second and transfer its energy to the most unstable mode. The conjecture is that when more than two unstable modes exist a similar mechanisms will concentrate all the energy in a single mode as well.

Once the amplitude is saturated and most of the energy (more than 99.9%) is concentrated into the most unstable mode the motion is nearly periodic. The results of performing a FFT using a sampling window of roughly 6 periods can be seen in figure 30. Notice that for the blade DoF the motion is nearly sinusoidal, with negligible presence of higher harmonics. On the other hand, the fir-tree DoF which is directly connected to the non-linear constraint shows significant values of the first odd harmonics. Using regression the best fitting for the blade frequency has been found to be 2.61% higher than the nominal vibration frequency.

Large Computational Domain

This case is identical to the six-sector model in the sense that both, the aerodynamic and structural parameters are the same, the sole difference is that we are including in the model thirty-six sectors that physically corresponds to 72 rotor blades welded in pairs instead of six. Since we have now more DoFs the dynamics of the problem is richer and more complex. The unsteady aerodynamics associated to this case is also that displayed in Fig. 31, however since in this configuration we may accommodate more modes we have consequently more unstable modes. Actually the forward traveling waves corresponding

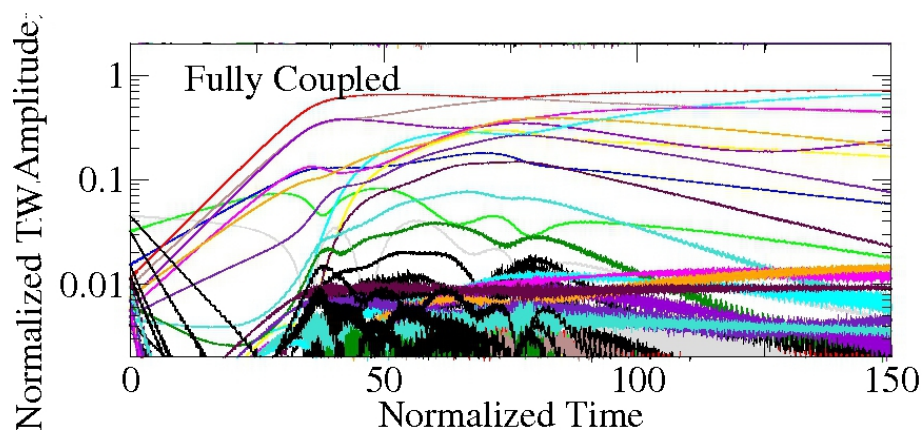


Figure 32: 36 SECTOR MODEL: TIME EVOLUTION OF THE TRAVELING WAVES

to the $ND = 2 - 13$, both included, are unstable. These twelve unstable modes have different critical damping ratio as it may be appreciated in Fig. 31.

The vibration amplitude of the airfoils saturates at nearly the same value than the model with six sectors. The same is true for the time needed to reach the amplitude saturation value. This effectively means that the growth rate of the instability in both cases is roughly the same, as could be expected, since the six-sector model contains nearly the most unstable mode.

Nevertheless, a more in depth analysis based on the tracking of the traveling-wave amplitudes (see Fig. 32) reveals that, even if the airfoil amplitudes have reached their final saturated value, there is still energy exchange among the different unstable waves. This is clearly seen between the non-dimensional time 100 and 150, where it may be appreciated that many modes are still active. Every line of Figs. 32 and 33 denotes the evolution of an aeroelastic mode (i.e.: a TW with a prescribed wave-length or ND). The colour code is consistent between both figures, unfortunately since every figure has 36 lines it is not appropriate to include the legends in them. The reader may pay attention to the colour code to compare the different figures.

The aerodynamic damping of the system obtained by two independent methods: (i) The RANS frequency domain linear solver prescribing the frequency that is obtained assuming that the non-linear contact is fixed (solid line) and (ii) The analysis of the first stages of the fully coupled non-linear method are very similar being the discrepancies associated to a slight shift of the vibration frequencies between the non-linear and the linear method and the non-linearity itself. The main conclusion is that the aerodynamics of the system is linear since the fully non-linear time marching method provides nearly the same results than the frequency domain linear methodology.

The results depicted in Fig. 32 are not fully satisfactory since they do not allow to conclude which is the final state of the system. Our conjecture, that we have already used in previous works [8, 9], is that the final state of a bladed-disk system with multiple unstable modes of the same family in the absence of a periodic forcing, includes just the most unstable mode. Because of the limited amount of simulation time the end time of Fig. 32 corresponds approximately to 150 periods.

The results obtained for characteristic times of the order of several thousands of periods may be seen in Fig. 33). It may be appreciated that for very long times just a single TW survives which, incidentally, was the one predicted as most unstable by the linear method (the forward TW of the 7th nodal diameter). This simulation, together with the one performed for the six-sector computational domain, confirms that the conjecture is true. The initial stages of the fully-non linear simulation are shown on the bottom of the same figure. It is seen that the dynamics is the same than that of the semi-uncoupled approach and the

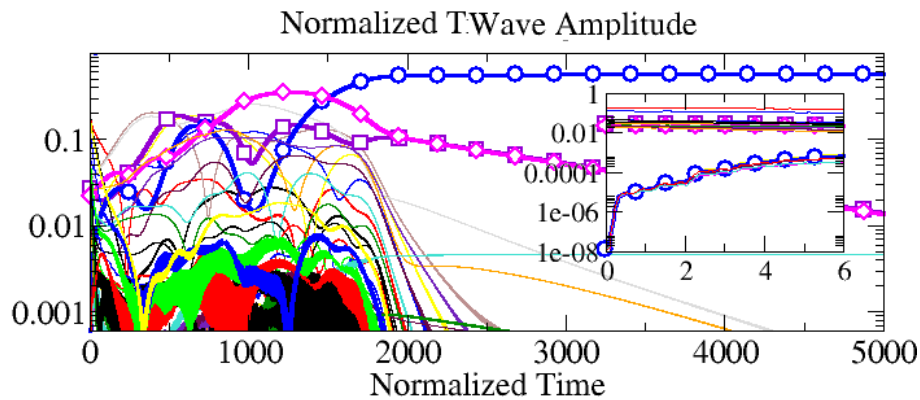


Figure 33: 36 SECTOR MODEL: LONG TIME EVOLUTION OF THE TRAVELING WAVES

non-linearity is filtering out the solution. There are clear indications that only a single model will survive in the long term. This simulation may be seen as a final indication that the conjecture that we formulated is true. Actually the most unstable mode, ND^* , was not perturbed at all while $ND = ND^* \pm 1$ were. However the dynamics select the most unstable mode although there were other very similar much larger at the initial stage.

Acknowledgments

I would like to thank here all the people that has contributed during many years to develop the understanding of Aeroelasticity both at Industria de Turbopropulsores S.A. and Universidad Politécnic de Madrid. This includes a large number of Master and Ph.D students and ITP research engineers. Among all of them I would like specially to thank Juan Manuel Gallardo that has been involved in the development of all the ITP aeroelasticity system from the very beginning. I am also in great debt with Carlos Vasco that developed the linear version of the aerodynamic suite of codes known as Mu^2s^2T .

References

- [1] Corral, R., Gallardo, J. M., and Martel, C., "A Conceptual Flutter Analysis of a Packet of Vanes Using a Mass-Spring Model," *Journal of Turbomachinery*, Vol. 131, April 2009, pp. 021016–1–7.
- [2] Antona, R., Corral, R., Gallardo, J., and Martel, C., "Effect of the Structural Coupling on the Flutter Onset of a Sector of Low-Pressure Turbine Vanes," *ASME Paper GT2010-23037*, Proceedings of the 55th ASME Gas Turbine and Aero engine Congress, Exposition and Users Symposium, Glasgow, UK, June 2010.
- [3] Corral, R., Gallardo, J., and Vasco, C., "Aeroelastic Stability of Welded-in-Pair Low Pressure Turbine Rotor Blades: A Comparative Study Using Linear Methods," *Journal of Turbomachinery*, Vol. 129, January 2007, pp. 72–83.
- [4] Zhai, Y., Bladh, R., and Dyverfeldt, G., "Mistuned Aeroelastic Stability Assessment of an Industrial Compressor Blade," *ASME Paper GT2011-45800*, Proceedings of the 56th ASME Gas Turbine and Aero engine Congress, Exposition and Users Symposium, Vancouver, Canada, June 2011.
- [5] Sinha, A. and Griffin, J. H., "Friction Damping of Flutter in Gas Turbine Engine Airfoils," *AIAA Journal of Aircraft*, Vol. 20, April 1983, pp. 372–376.

-
- [6] Sinha, A. and Griffin, J. H., "Effects of Friction Dampers on Aerodynamically Unstable Rotor Stages," *AIAA Journal*, Vol. 23, No. 2, Feb 1985, pp. 262–270.
- [7] Midlin, R. D. and Deresiewicz, H., "Elastic Spheres in Contact Under Varying Oblique Forces," *Journal of Applied Mechanics*, Vol. 20, 1953, pp. 327–344.
- [8] Corral, R. and Gallardo, J. M., "A Methodology for the Vibration Amplitude Prediction of Self-Excited Rotors Based on Dimensional Analysis," *ASME Paper 20005-GT-90668*, Proceedings of the 51st ASME Gas Turbine and Aero engine Congress, Exposition and Users Symposium, Barcelona, Spain, May 2006.
- [9] Corral, R. and Gallardo, J., "Verification of the Vibration Amplitude Prediction of Self-Excited LPT Rotor Blades Using a Fully Coupled Time-Domain Non-Linear Method and Experimental Data," *ASME Paper 2008-GT-51416*, Proceedings of the 51st ASME Gas Turbine and Aero engine Congress, Exposition and Users Symposium, Berlin, Germany, June 2008.
- [10] Corral, R. and Gallardo, J., "Non-Linear Dynamics of Multi-Mode Unstable Bladed-Disks: Part I - Description of a Canonical Model and Phenomenological Results," *ASME Paper GT2011-22943*, Proceedings of the 56th ASME Gas Turbine and Aero engine Congress, Exposition and Users Symposium, Vancouver, Canada, June 2011.